Relationship between tectonic overpressure, deviatoric stress, driving force, isostasy and gravitational potential energy

Stefan M. Schmalholz,[1] Sergei Medvedev,[2] Sarah M. Lechmann[3,*] and Yuri Podladchikov[1]

[1]*Institute of Earth Sciences, University of Lausanne, Lausanne, Switzerland. E-mail: stefan.schmalholz@unil.ch*
[2]*Centre for Earth Evolution and Dynamics, University of Oslo, Oslo, Norway*
[3]*Geological Institute, ETH Zurich, Zurich, Switzerland*

SUMMARY

We present analytical derivations and 2-D numerical simulations that quantify magnitudes of deviatoric stress and tectonic overpressure (i.e. difference between the pressure, or mean stress, and the lithostatic pressure) by relating them to lateral variations in the gravitational potential energy (*GPE*). These predictions of tectonic overpressure and deviatoric stress associated with *GPE* differences are independent of rock rheology (e.g. viscous or elastic) and rock strength. We consider a simple situation with lowlands and mountains (plateau). We use a numerical two-layer model consisting of a crust with higher Newtonian viscosity than that in the mantle, and also a three-layer model in which the two-layer lithosphere overlies a much less viscous asthenosphere. Our results (1) explain why estimates for the magnitude of stresses in Tibet, previously published by different authors, vary by a factor of two, (2) are applied to test the validity of the thin sheet approximation, (3) show that the magnitude of the depth-integrated tectonic overpressure is equal to the magnitude of the depth-integrated deviatoric stress if depth-integrated shear stresses on vertical and horizontal planes within the lithosphere are negligible (the thin sheet approximation) and (4) show that under thin sheet approximation tectonic overpressure is required to build and support continental plateaus, such as in Tibet or in the Andes, even if the topography and the crustal root are in isostatic equilibrium. Under thin sheet approximation, the magnitude of the depth-integrated tectonic overpressure is equal to the depth-integrated horizontal deviatoric stress, and both are approximately 3.5×10^{12} N m^{-1} for Tibet. The horizontal driving force per unit length related to lateral *GPE* variations around Tibet is composed of the sum of both tectonic overpressure and deviatoric stress, and is approximately 7×10^{12} N m^{-1}. This magnitude exceeds previously published estimates for the force per unit length required to fold the Indo-Australian Plate south of India, and hence the uplift of the Tibetan plateau could have folded the Indian Plate. We also discuss the mechanical conditions that are necessary to achieve isostasy, for which the lithostatic pressure is constant at a certain depth. The results show that tectonic overpressure can exist at a certain depth even if all deviatoric stresses are zero at this depth, because this tectonic overpressure is related to horizontal gradients of vertical shear stresses integrated across the entire depth of the lithosphere. The magnitude of the depth-integrated tectonic overpressure of 3.5×10^{12} N m^{-1} implies that the pressure estimated from observed mineral assemblages in crustal rocks is likely significantly different from the lithostatic pressure, and pressure recorded by crustal rocks is not directly related to depth. In case of significant weakening of the entire lithosphere by any mechanism our analytical and numerical studies provide a simple estimation of tectonic overpressure via variations in *GPE*.

Key words: Continental tectonics: compressional; Continental tectonics: extensional; Dynamics of lithosphere and mantle; Dynamics: gravity and tectonics; Mechanics, theory, and modelling.

*Now at: armasuisse, Federal Department of Defence, Civil Protection and Sport, Thun, Switzerland.

GJI Geodynamics and tectonics

INTRODUCTION

Quantifying stresses in the lithosphere is important to constrain the forces that drive plate tectonics and to define the style of lithospheric deformation. Understanding the distribution of pressure (mean stress) within the lithosphere is furthermore important because geodynamic reconstructions can be calibrated by pressure estimations from observed mineral assemblages in exhumed rocks. In this study, we address two fundamental questions: (1) what is the magnitude of pressure in the lithosphere around long-lived continental plateaus? and (2) what is the relation between pressure, deviatoric stress and the density structure of the lithosphere?

The lithostatic pressure is the pressure resulting only from the mass of the overburden rock and is equivalent to the hydrostatic pressure in fluids at rest. The lithostatic pressure is calculated by vertically integrating the density profile of the overburden rock (multiplied by the gravitational acceleration). The relation between the lithostatic pressure and the stresses within a deforming lithosphere, however, is not trivial, and is one of the topics of this study. Depth-integrated lithostatic pressure is often termed gravitational potential energy (*GPE*, e.g. Molnar & Lyon-Caen 1988; Jones *et al.* 1996; Ghosh *et al.* 2006, 2009). The integration boundaries are the Earth surface and the base of the lithosphere. It is usually assumed that the lithosphere is in isostatic equilibrium at its lower boundary that is defined as a 'compensation depth'.

Horizontal variations in *GPE* have been used to estimate absolute magnitudes of the depth-integrated horizontal stress or the horizontal force per unit length in the lithosphere (e.g. Artyushkov 1973; Parsons & Richter 1980; Molnar & Lyon-Caen 1988; Ghosh *et al.* 2006). These estimates are of particular interest, because (1) the calculated values of the *GPE* depend only on the density variation in the lithosphere and mantle and are, therefore, relatively robust, and (2) the stress estimates can be calculated directly from the force balance equations, and they may, as we explain here, be independent of any assumptions concerning the rock rheology (e.g. viscous or elastic) and the rock strength.

Horizontal stress estimates from *GPE* variations are either calculated by using simple analytical relations (e.g. Artyushkov 1973; Dalmayrac & Molnar 1981; Molnar & Lyon-Caen 1988) or by using thin viscous sheet models, because the governing equations of thin viscous sheet models include the horizontal derivatives of the *GPE* (e.g. Bird & Piper 1981; England & McKenzie 1982, 1983; England & Houseman 1986; Houseman & England 1986; England & Molnar 1997; Flesch *et al.* 2001; Ghosh *et al.* 2009). However, based on the same *GPE* data different estimates of stress magnitudes have been presented in previous studies. For example, Flesch *et al.* (2001) and Ghosh *et al.* (2006, 2009, 2013) estimated stress magnitudes for Tibet using thin viscous sheet models, and they argue that stress magnitudes for Tibet inferred from an analytical relation applied by Molnar & Lyon-Caen (1988) and Molnar *et al.* (1993) are a factor of two larger than stress magnitudes provided by their thin viscous sheet models. Ghosh *et al.* (2006, 2009) argue that Molnar and coauthors overestimate stress magnitudes in Tibet, and that this overestimation results from (1) a 2-D approximation of the 3-D lithosphere, (2) an unconventional definition of the deviatoric stress and (3) assigning pressure to lithostatic pressure. In this study, we explain why previously published stress estimates vary by a factor of two, and show that estimates of Molnar and coauthors (1988, 1993) use less simplified assumptions than presumed in the later studies.

Previous studies have applied *GPE* variations mainly to estimate magnitudes of stress and only few studies discussed the magnitudes

of pressure (e.g. Naliboff *et al.* 2012). In particular, the magnitude of the tectonic overpressure (i.e. the difference between the pressure, or mean stress, and the lithostatic pressure; e.g. Mancktelow 2008) was not linked before to *GPE*. However, quantifying the tectonic overpressure is important for the reconstruction of the tectonic evolution of mountain belts and continental plateaus using pressure–temperature (P-T) paths constructed from mineral assemblages observed in the field. Usually, P-T studies assume that the pressure is equal to the lithostatic pressure (e.g. Schreyer 1995) and, therefore, pressure is often directly converted into a burial depth assuming typical densities for the crust and mantle (e.g. Ernst 2001). Such depth estimates resulting from the assumption that pressure equals lithostatic pressure are frequently one of the main arguments for proposed geodynamic scenarios, such as deep subduction of continental crust (e.g. Jolivet *et al.* 2003) or rapid exhumation of rock from great depth (e.g. Rubatto & Hermann 2001). In this study, we show that *GPE* variations can also be used to estimate absolute magnitudes of tectonic overpressure. We present both analytical derivations and simple 2-D numerical simulations to explain and quantify the relationship between lateral *GPE* variations, tectonic overpressure and deviatoric stress within the lithosphere.

In this study, we also discuss two concepts used for describing the state of stress at the base of, or below, the lithosphere, namely, compensation and isostasy. The difference between these two concepts is important for our study. Throughout the paper we assume that the base of the lithosphere and/or underlying asthenosphere is much weaker than the shallower regions of the lithosphere and that deviatoric stresses around the base of our model are vanishingly small. The depth around which we neglect deviatoric stresses is termed the depth of compensation. Negligible deviatoric stresses imply that the pressure (mean stress) is constant along the compensation depth and the condition of constant pressure is referred to as compensation condition (Table 1). If additionally the lithostatic pressure is constant along the compensation depth, then we use the term isostasy to describe the local type of isostasy (Table 1). Therefore, the terms compensation and isostasy represent here different mechanical conditions and we will demonstrate that these conditions may exclude each other.

RHEOLOGY-INDEPENDENT ANALYTICAL RESULTS

This section presents a set of relations between depth-integrated stresses (denoted by an overbar, Table 1) that are simply related to the depth-averaged stress values (depth-integrated values are equal to the depth-averaged values times the corresponding thickness). Working with depth-integrated quantities requires a special attention on the physical units since the depth-integrated stress has units of Pa·m (or N m^{-1}), whereas stress has units of Pa (Table 1).

For simplicity only the 2-D case is considered here. According to the definitions given in the 'Introduction' section the lithostatic pressure, P_L, is defined as

$$P_L(x, z) = \int_z^{St(x)} \rho(x, z') g \, dz', \tag{1}$$

and the *GPE* (in units of Pa·m or N m^{-1}) is defined as

$$GPE(x) = \int_{Sb}^{St(x)} P_L(x, z) \, dz + \text{const}, \tag{2}$$

where x is the horizontal coordinate, z the vertical coordinate, ρ is the density, g the gravitational acceleration and Sb and $St(x)$ represent the constant compensation depth and the laterally varying

Table 1. Summary of key symbols, their explanations and related equations.

Symbol	Explanation	Related equation
$St(x)$, Sb	Topography, $St(x)$, is variable in the horizontal x-direction and the model base, Sb, is constant in the x-direction.	
σ, τ and P	Total stresses, deviatoric stresses and pressures, respectively, in units of N m^{-2} (or Pa). σ, τ and P are function of x and z.	$\sigma_{xx} = \tau_{xx} - P, \qquad \sigma_{xz} = \tau_{xz}$ $\sigma_{zz} = \tau_{zz} - P, \qquad \tau_{xx} + \tau_{zz} = 0$
Q	Integrated measure of the shear stress, σ_{xz}, in units of N m^{-2} (or Pa). Q is a function of x and z.	$Q(x,z) = \frac{\partial}{\partial x} \int_z^{St(x)} \sigma_{xz}\, dz\prime$
P_L	Lithostatic pressure in units of N m^{-2} (or Pa). P_L is function of x and z.	$P_L(x,z) = \int_z^{St(x)} \rho(x,z\prime)\, g\, dz\prime$
P_O	Tectonic overpressure in units of N m^{-2} (or Pa). P_O is function of x and z.	$P_O(x,z) = P(x,z) - P_L(x,z)$
$\bar{\sigma}$, $\bar{\tau}$, $\bar{P}$ and $\bar{Q}$	The overbar indicates the vertical integral of the respective quantity and overbarred quantities have units of N m^{-1} (or Pa·m). Overbarred terms are only function of x. Note that overbarred quantities have the same unit as the *GPE*.	e.g. $\bar{\sigma}(x) = \int_{Sb}^{St(x)} \sigma(x,z)\, dz$
GPE	Gravitational potential energy, in units of N m^{-1} (or Pa·m). *GPE* is only function of x.	$GPE(x) = \int_{Sb}^{St(x)} P_L(x,z)\, dz + \text{const}$
F_x	Horizontal driving force per unit length in units of N m^{-1} (or Pa·m), the integrated difference between the total stress, σ_{xx} and a hydrostatic stress, $\sigma_{xx}^s = -P_L$. F_x is only function of x.	$F_x(x) = \overline{\sigma_{xx}(x,z) + P_L(x,z)}$
Δ	Difference between values at different horizontal locations.	e.g. $\Delta\sigma_{zz} = 0 \Leftrightarrow \frac{\partial}{\partial x}\sigma_{zz} = 0$

upper surface of the crust, respectively (see also Fig. A1 and Table 1). Using a stress-free upper surface and zero shear stress at the model bottom (representing the compensation depth) as boundary conditions, the depth-integrated horizontal force balance in 2-D reduces to the exact equality (e.g. Dalmayrac & Molnar 1981; Molnar & Lyon-Caen 1988; Medvedev & Podladchikov 1999a,b; see eqs A1–A8):

$$\frac{\partial}{\partial x}\left(\bar{\sigma}_{xx}\right) = 0, \tag{3}$$

where σ_{xx} is the horizontal stress (in units of Pa), and the bar on top of a symbol indicates the vertical integral of the symbol (Table 1). Therefore, the units of $\bar{\sigma}_{xx}$ are Pa·m or N m^{-1}, the overbarred quantities have the same units as the *GPE* and overbarred quantities can be considered as a force per unit length (Table 1). It follows from eq. (3) that $\bar{\sigma}_{xx}$ is constant in the horizontal x-direction. Eq. (3) is modified by adding the horizontal derivative of eq. (2) which yields

$$\frac{\partial}{\partial x}\left(\bar{\sigma}_{xx} + \bar{P}_L\right) = \frac{\partial}{\partial x}(GPE). \tag{4}$$

No assumptions have been made so far concerning the shear stress distribution within the lithosphere or the condition of isostasy at the compensation depth. Eq. (4) shows that the horizontal variation in *GPE* is related to the horizontal variation of $\bar{\sigma}_{xx} + \bar{P}_L$. $\bar{\sigma}_{xx}$ can be decomposed into a depth-integrated pressure, $\bar{P}$, and a depth-integrated horizontal deviatoric stress, $\bar{\tau}_{xx}$:

$$\bar{\sigma}_{xx} = -\bar{P} + \bar{\tau}_{xx}. \tag{5}$$

The depth-integrated tectonic overpressure, $\bar{P}_O$, is the difference between the depth-integrated pressure and the depth-integrated lithostatic pressure, that is, $\bar{P}_O = \bar{P} - \bar{P}_L$. Substituting $\bar{P} = \bar{P}_L + \bar{P}_O$ and eq. (5) into (4) yields

$$\frac{\partial}{\partial x}\left(-\bar{P}_O + \bar{\tau}_{xx}\right) = \frac{\partial}{\partial x}(GPE). \tag{6}$$

If $\bar{P}_O$ were equal to zero, then the variations in *GPE* would be directly related to variations in $\bar{\tau}_{xx}$. However, zero tectonic overpressure is equivalent to the condition that pressure is equal to the lithostatic pressure, which can occur only when no deformation takes place in the system. However, no deformation implies that the deviatoric stress is zero, and thus the *GPE* should be constant. If lateral variations of the geometry of the lithosphere are observed, then the *GPE* cannot be constant. Therefore, eq. (6) states that the lateral variation in *GPE* requires the same variation in the sum of the depth-integrated tectonic overpressure and deviatoric stress. Consequently, at least one of the two quantities is not negligible, and tectonic overpressure and deviatoric stress cannot be negligibly small at the same time (note that assuming that pressure is equal to the lithostatic pressure actually implies that both overpressure and deviatoric stress are negligible). Numerical simulations presented in a later section confirm that for typical model configurations with mountains and lowlands (Fig. 1) a considerable tectonic overpressure always exists and is of the same order as $\bar{\tau}_{xx}$ (see also eq. A12).

Molnar & Lyon-Caen (1988) used eq. (4) to estimate the driving horizontal force per unit length, F_x, that is derived from the difference between the actual horizontal total stress, $\bar{\sigma}_{xx}$, and the static horizontal total stress, $\bar{\sigma}_{xx}^s = -\bar{P}_L$:

$$\frac{\partial}{\partial x}(F_x) = \frac{\partial}{\partial x}\left(\bar{\sigma}_{xx} - \bar{\sigma}_{xx}^s\right) = \frac{\partial}{\partial x}\left(\bar{\sigma}_{xx} + \bar{P}_L\right) = \frac{\partial}{\partial x}\left(-\bar{P}_O + \bar{\tau}_{xx}\right)$$

$$= \frac{\partial}{\partial x}(GPE). \tag{7}$$

(a) Two-layer model (not to scale)
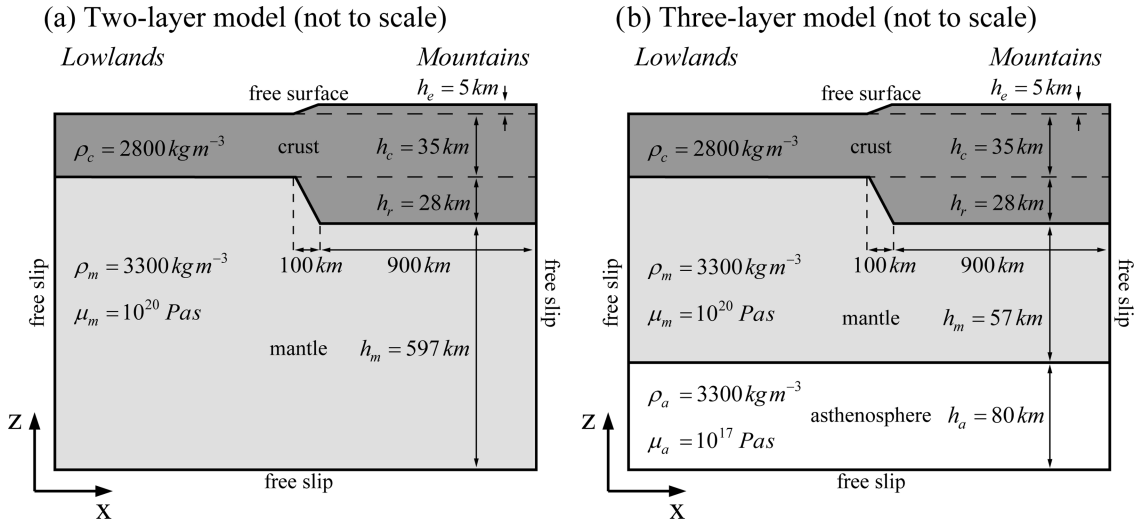

(b) Three-layer model (not to scale)

Figure 1. Model configuration for the two-layer (a) and three-layer (b) model, and parameters that are identical for most (exceptions are mentioned in the text) simulations. ρ_c, ρ_m, ρ_a, μ_m, μ_a, h_e, h_c, h_r, h_m and h_a are the density of the crust, the density of the mantle, the density of the asthenosphere, the viscosity of the mantle, the viscosity of the asthenosphere, the initial elevation of the mountains, the initial thickness of the crust, the initial thickness of the root below the mountains, the initial thickness of the mantle below the mountains and the thickness of the asthenosphere, respectively. Vertical, lateral boundaries are fixed and do not move horizontally.

Using $P_O = -\tau_{xx} + Q$ (eq. A12), where Q represents the influence of the shear stresses (eq. A11), eq. (6) can be rewritten as

$$\frac{\partial}{\partial x}(GPE) = \frac{\partial}{\partial x}\left(2\bar{\tau}_{xx} - \overline{Q}\right) \overset{TS}{\approx} \frac{\partial}{\partial x}\left(2\bar{\tau}_{xx}\right) \overset{TS}{\approx} \frac{\partial}{\partial x}\left(2\bar{P}_O\right), \quad (8)$$

where '*TS*' above the approximate equal sign indicates one of the main simplifications of the thin sheet approximation, which is the vanishing influence of the shear stresses, represented by Q (Table 1), in the integrated stress balance (e.g. England & McKenzie 1982, 1983). However, in contrast to the 'traditional' derivation of the thin sheet equations, which assumes zero shear stress, σ_{xz}, throughout the entire sheet, eq. (8) is valid for a much weaker assumption, namely, $\overline{Q} = $ const. Numerical simulations presented in the next section demonstrate that ignoring Q may indeed be valid and estimates are accurate to a certain degree. Combining eqs (7) and (8) yields

$$\frac{\partial}{\partial x}(GPE) = \frac{\partial}{\partial x}(F_x) \overset{TS}{\approx} \frac{\partial}{\partial x}\left(2\bar{\tau}_{xx}\right). \quad (9)$$

Eq. (9) shows that estimates of the driving horizontal force F_x, calculated by Molnar & Lyon-Caen (1988), are indeed approximately twice (or exactly twice if $\overline{Q} = 0$) larger than estimates of the integrated deviatoric stress, $\bar{\tau}_{xx}$, presented by Flesch *et al.* (2001) and Ghosh *et al.* (2006, 2009, 2013). Therefore, there is no contradiction (controversy may still exist) between these two estimates of F_x and $\bar{\tau}_{xx}$. However, one should mention that whereas the estimates of F_x are exact, estimates of $\bar{\tau}_{xx}$ are based on the assumption of vanishing influence of shear stress within the lithosphere. Therefore, if during the deformation of the lithosphere the shear stress contribution Q is not negligible, the thin sheet approximation in eq. (9) may become inaccurate. For example, the thin sheet approximation is incorrect where flexure occurs (e.g. Molnar & Lyon-Caen 1988), and during large-scale folding, both at the onset of the folding instability due to the importance of flexural moments (e.g. Medvedev & Podladchikov 1999a,b; Schmalholz *et al.* 2002) and at the later stages of folding due to the control of $\bar{\tau}_{xx}$ by the layer length, which is not captured by the thin sheet approximation (Schmalholz & Podladchikov 2000).
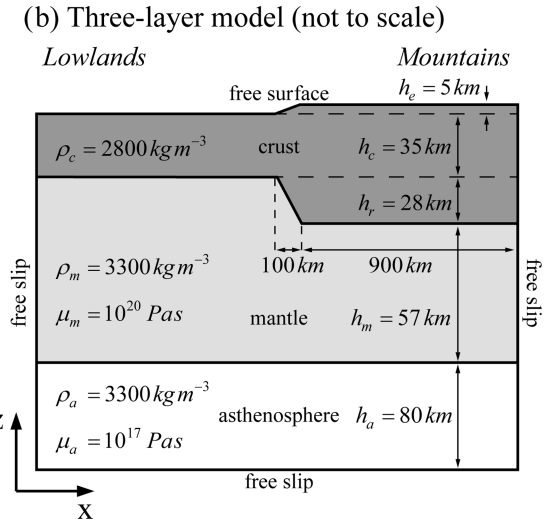
If we use the *GPE* of the lowlands as reference value, then the difference in *GPE*, ΔGPE, due to a variation of the elevation, h_e, and the root of the crust, h_r, in the mountains is (Fig. 1):

$$\Delta F_x = \Delta\left(-\bar{P}_O + \bar{\tau}_{xx}\right) = \Delta GPE. \quad (10)$$

Eq. (10) shows that differences in *GPE* between lowlands and mountains are related to differences in F_x and in $-\bar{P}_O + \bar{\tau}_{xx}$. We present next an expression for the *GPE* difference directly resulting from its definition in eq. (2), without assuming isostasy:

$$\Delta F_x = \Delta GPE = \rho_c g h_e\left(\frac{h_e}{2} + h_c + h_r + h_m\right)$$
$$- (\rho_m - \rho_c)g h_r\left(\frac{h_r}{2} + h_m\right), \quad (11)$$

where ρ_c and ρ_m are the density of the crust and the density of the mantle, respectively, h_c and h_m are the thickness of the crust in the lowlands and the thickness of the mantle above the depth of compensation (below the mountains), respectively (Fig. 1). Eq. (11) is valid for any crustal/lithosphere geometry, and will be used to calculate ΔF_x using crustal geometries resulting from numerical simulations (described in a later section), which do not include the isostasy condition. The value of ΔF_x in eq. (11) depends on the assumed depth of compensation. This depth dependency disappears if the system is in the state of isostasy. Using isostasy ($\Delta P_L = 0$ along the compensation depth), the ΔGPE can be split into two parts, namely, an isostatic part (with subscript 'iso') that quantifies the ΔGPE assuming that the topographic elevation, h_e, is supported isostatically by the root of the crust, h_r, and a non-isostatic part (with subscript 'non-iso'):

$$\Delta GPE = \Delta GPE_{\text{iso}} + \Delta GPE_{\text{non-iso}},$$
$$\Delta GPE_{\text{iso}} = \rho_c g h_e\left(h_c + \frac{\rho_m}{\rho_m - \rho_c}\frac{h_e}{2}\right),$$
$$\Delta GPE_{\text{non-iso}} = \Phi g\left(h_m + \frac{h_r}{2} - \frac{\rho_c}{\rho_m - \rho_c}\frac{h_e}{2}\right), \quad (12)$$

with $\Phi = \rho_c h_e - (\rho_m - \rho_c) h_r$.

If the lithosphere is in the state of isostasy, the topographic elevation and crustal roots are related to each other by $\rho_c h_e = (\rho_m - \rho_c) h_r$, and $\Delta GPE_{\text{non-iso}} = 0$, because $\Phi = 0$. Consequently, ΔGPE is only controlled by ΔGPE_{iso}. Using ΔGPE_{iso} instead of ΔGPE has some advantages, because ΔGPE_{iso} is independent of the depth of integration (usually, an arbitrary chosen depth of compensation) and requires knowledge of only topographic elevation, h_e, and crustal thickness, h_c. However, the application of ΔGPE_{iso} assumes isostasy, which may limit the applicability to certain natural cases. Therefore, we discuss next the conditions necessary for isostasy.

In general, the deviation from isostasy expressed by the variation of the lithostatic pressure, ΔP_L, at the compensation depth is related to variations in the horizontal derivative of the depth-integrated shear stress (see eq. A17 and its derivation in the Appendix):

$$\Delta Q = \Delta \left(\frac{\partial}{\partial x} \bar{\sigma}_{xz} \right) = -\Delta P_L = \Delta P_O. \tag{13}$$

Far away from the topographic gradient at the boundary between mountains and lowlands, the depth-integrated shear stress is negligible because of vanishing horizontal gradients of the lithospheric structure. Eq. (13) implies that the vertical integral of the shear stresses σ_{xz} through the entire lithosphere should be zero everywhere so that the condition of local isostasy (i.e. $\Delta P_L = 0$) can be fulfilled everywhere at the compensation depth. Consequently, the condition of local isostasy is based on a stronger assumption, namely, that shear stresses are zero throughout the entire lithosphere, than the condition of compensation, namely, that deviatoric stresses are zero only within a finite layer around the depth of compensation. In the region around the boundary between mountains and lowlands, where most of the deformation takes place, the horizontal gradients of depth-integrated shear stresses are likely not negligible, and the assumption of local isostasy is likely not applicable. Therefore, eq. (11) is more accurate than eq. (12) for quantifying (1) values of ΔGPE and (2) variations of ΔGPE in regions with topographic gradients. In a later section we confirm the higher accuracy of eq. (11) with 2-D numerical results and estimate the potential error of using the isostatic approach to GPE.

Applications of eq. (12) to the analysis of real lithospheric stresses, however, are limited. On one hand, the exact integration of eq. (2) requires precise knowledge of the density structure of the lithosphere, which is rarely available. On the other hand, the non-isostatic part of the GPE variations, $\Delta GPE_{\text{non-iso}}$, is proportional to h_m (eq. 12), which is considerably larger than any length scales appearing in ΔGPE_{iso}. Large deviations from isostasy would be further amplified by large values of h_m within $\Delta GPE_{\text{non-iso}}$, and consequently may require extreme magnitudes of the driving force, F_x (eq. 10). Thus, even though deviations from the local isostasy in the Earth's lithosphere are likely, this deviation should not be considerably large.

RHEOLOGY-DEPENDENT ANALYTICAL RESULTS

Next, we estimate the distribution and magnitudes of deviatoric stresses and tectonic overpressure within a simple model of a two-layer lithosphere (Fig. 1a). The lateral model boundaries are fixed and there is no horizontal shortening or extension of the model domain. Therefore, deformation only occurs because of the variations

in GPE inside the model domain. Assuming that $\bar{Q}$, the integrated measure of the shear stress, is negligible (or constant), eq. (8) yields

$$\Delta \bar{\tau}_{xx} \approx -\Delta \bar{P}_O \approx \frac{1}{2} \Delta GPE. \tag{14}$$

We apply one more assumption that is usually used in the thin sheet approximations, namely, that the horizontal velocity does not vary with depth. We, therefore, kinematically restrict the lithospheric deformation to pure shear only. This assumption implies that horizontal strain rates are only a function of x, which can be expressed as

$$\frac{\tau_{xx}}{\mu} = f(x), \tag{15}$$

where $\mu = \mu(x, z)$ is the viscosity. Separating stresses and viscosities in the crust (with sub- or superscript 'c') and in the mantle (with sub- or superscript 'm') within our test model (Fig. 1a), we can write

$$\frac{\tau_{xx}^m}{\mu_m} = \frac{\tau_{xx}^c}{\mu_c} = f(x). \tag{16}$$

At a specific x-position we can write

$$\tau_{xx}^m = \frac{\mu_m}{\mu_c} \tau_{xx}^c. \tag{17}$$

Integrating τ_{xx} vertically yields

$$\bar{\tau}_{xx} = \left(h_c + \frac{\mu_m}{\mu_c} h_m \right) \tau_{xx}^c = \frac{\mu_c h_c + \mu_m h_m}{\mu_c} \tau_{xx}^c. \tag{18}$$

Considering the model configuration in Fig. 1(a), the difference in depth-integrated horizontal deviatoric stresses in the crust between lowlands and mountains is

$$\Delta \bar{\tau}_{xx} = \frac{\mu_c (h_c + h_e + h_r) + \mu_m (h_m - h_r)}{\mu_c} \tau_{xx}^c \big|_{\text{Mountains}}$$
$$- \frac{\mu_c h_c + \mu_m h_m}{\mu_c} \tau_{xx}^c \big|_{\text{Lowlands}} . \tag{19}$$

Assuming that $\mu_c h_c \gg \mu_m h_m$ (or $\mu_c / \mu_m \gg h_m / h_c$) and substituting eq. (19) into (14) yields

$$\Delta \bar{\tau}_{xx} \approx -\Delta \bar{P}_O \approx \frac{1}{2} \Delta GPE \approx (h_c + h_e + h_r) \tau_{xx}^c \big|_{\text{Mountains}}$$
$$- h_c \tau_{xx}^c \big|_{\text{Lowlands}} . \tag{20}$$

Furthermore, for our model configuration with fixed lateral boundaries and without far-field tectonic background stress the lowlands are under compression and the mountains are under extension. Considering the special case of $\tau_{xx}^c \big|_{\text{Mountains}} \approx - \tau_{xx}^c \big|_{\text{Lowlands}}$, eq. (20) provides a rough estimate for the magnitude of the crustal deviatoric stress (and also for the tectonic overpressure) in the lowlands and the mountains as function of ΔGPE:

$$\tau_{xx}^c \approx -P_O^c \approx \frac{\Delta GPE}{2 (2h_c + h_e + h_r)}. \tag{21}$$

Eq. (21) provides a viscosity-independent lower bound for the magnitudes of crustal deviatoric stress and tectonic overpressure for the condition $\mu_c / \mu_m \gg h_m / h_c$. For a given value of ΔGPE a combination of eqs (14) and (19) provides the relation between characteristic magnitudes of τ_{xx}^c (or P_O^c) within the crust of the lowlands and the mountains. The estimation of specific magnitudes of $\tau_{xx}^c \big|_{\text{Mountains}}$ and $\tau_{xx}^c \big|_{\text{Lowlands}}$ seems not possible with our simple analytical model, but the relation between the stresses provides additional information on the stress magnitudes in the lowlands and

the mountains. Substituting eq. (14) into (19), rearranging the terms and introducing the viscosity ratio, $R = \mu_c / \mu_m$, provides

$$\tau_{xx}^c \big|_{\text{Lowlands}}$$

$$\approx \frac{\left[(h_c + h_e + h_r) + (h_m - h_r)/R\right] \tau_{xx}^c \big|_{\text{Mountains}} - \Delta GPE/2}{\left[h_c + h_m/R\right]}.$$

(22)

For a range of magnitudes of $\tau_{xx}^c \big|_{\text{Mountains}}$, the above equation provides the corresponding magnitudes of $\tau_{xx}^c \big|_{\text{Lowlands}}$ for a specific crustal geometry (given all the thicknesses), a specific density structure (which then determines ΔGPE) and a specific viscosity ratio between crust and mantle (R). Eq. (22) can equally be used to predict the relation for the tectonic overpressure. The stress relation of eq. (22) is displayed in Fig. 2(a) for three different values of R and the model configuration displayed in Fig. 1(a) (i.e. $h_m = 597$ km). In Fig. 2(b), the stress relation of eq. (22) is displayed for a lithospheric thickness of only 120 km (i.e. $h_m = 57$ km), corresponding to the configuration in Fig. 1(b) and for $R = 10$ and 100. The stress relation (22) has been plotted using the natural limits for the stresses for our model configuration (Fig. 1), namely, that the mountains are in a state of tension (here positive values of τ_{xx}^c), while the lowland is subjected to compression (here negative values of τ_{xx}^c). The analytical result for $R = 1000$ (for equal absolute stress magnitudes in lowlands and mountains) is close to the limit of $R \gg h_m/h_c$ and thus represents the rheology-independent lower bound for stress magnitudes predicted by eq. (21). The analytical prediction of absolute magnitudes of stress and tectonic overpressure using eq. (22) is based on the thin sheet approximation, and these predictions will be compared with results of 2-D numerical simulations in the next section.

NUMERICAL MODEL AND RESULTS

We solve the 2-D continuum mechanics force balance equations with the finite element method. We use a mixed formulation with Crouzeix–Raviart triangles with quadratic velocity shape functions enhanced by a cubic bubble function and discontinuous linear interpolation for the pressure field (so-called P2 $\pm$ P1 element, e.g. Thomasset 1981). We consider incompressible linear viscous fluids and apply the penalty method in combination with Uzawa iterations to enforce a divergence-free velocity field. A Lagrangian approach is used, and the numerical mesh is generated with the mesh generator Triangle (Shewchuk 2002). The model geometry is described through external and internal interfaces with 2001 nodes on a single-layer interface. Both the finite element mesh and the interfaces are moved with the resulting velocity fields. The applied finite element algorithm is described in more detail in Schmalholz *et al.* (2008) and Schmalholz & Schmid (2012), and relies on the fast finite element method solver MILAMIN (Dabrowski *et al.* 2008).

We consider two model configurations: a simplest two-layer model and a three-layer model mimicking the crustal and mantle lithosphere that overlies a much less viscous asthenopshere (Fig. 1). For both models, the lateral and the bottom boundaries are free-slip boundaries and the top boundary is a free surface. The lateral boundaries do not move and there is no horizontal shortening or extension of the model domain. The flow within the model domain results only from lateral variations of the *GPE* inside the model domain. The parameters that are the same for most (exceptions are mentioned explicitly) of the performed simulations are displayed in Fig. 1. The initial elevation and the root of the mountains agree with local isostasy, that is, $\rho_c h_e = (\rho_m - \rho_c) h_r$. The viscosity of the mantle is 10^{20} Pa·s in both models, and the viscosity of the asthenosphere in the three-layer model is 10^{17} Pa·s. The initial thickness of the two-layer model at the lowlands is 660 km to minimize the influence of the bottom free-slip boundary condition on the results. In the three-layer model, the horizontal boundary between the mantle and the asthenosphere is in a depth of 120 km (below the lowlands), and the asthenospheric layer extends from a depth of 120 km to the model bottom at a depth of 200 km, that is, the model asthenosphere is 80 km thick.

The results of six simulations of the two-layer model are presented in Figs 3–5. In three simulations, the viscosity of the crust was different with values of 10^{21}, 10^{22} and 10^{23} Pa·s (i.e. $R = 10$, 100 and 1000, respectively) and the width of the lowland was 1000 km (Figs 3a–c). In the three other simulations, the viscosity of the crust was 10^{22} Pa·s (i.e. $R = 100$) but the width of the lowland was different with values of 250, 500 and 750 km.

The horizontal deviatoric stress, τ_{xx}, is displayed in Fig. 3 for the 6 two-layer simulations and for the initial geometry (Fig. 1a). The results show that the distributions and magnitudes of τ_{xx} are different for all six simulations although the initial ΔGPE is identical. The magnitudes of stress depend on the viscosity of the crust (Figs 3a–c) and on the width of the lowlands (Figs 3d–f). Fig. 3(c) shows that absolute magnitudes of τ_{xx} are the same in the lowlands and the mountains despite the different crustal thickness. For the configuration of Fig. 3(c) ($R = 1000$) values of τ_{xx} in the lowlands and the mountains are accurately predicted by eq. (21) (Fig. 2a).

If lowlands and mountains have the same width, then this movement generates equal magnitudes of horizontal strain rates in the lowland and mountains. If, however, the width of the lowland region is significantly narrower than the mountains, then the strain rates in the lowlands are higher than in the mountains, and correspondingly stress is higher in the lowlands (Fig. 3). To qualitatively understand the rates of deformation in the system, one should consider the final phase of the deformation close to the static configuration, when the crustal thickness of the lowland and of the mountains becomes equal, and the variations of the topography (and *GPE*) become negligible. For the models with equal crustal width in the lowlands and the mountains (Figs 3a–c), the static configuration of the crust (i.e. constant thickness everywhere) is equally far away from the initial configuration in the lowlands and the mountains. Therefore, we should expect similar strain rates and deviatoric stresses in the lowlands and the mountains. The static configuration in the simulations with different crustal width (Figs 3d–f) is further away from the initial configuration in the lowlands. Therefore, magnitudes of strain rates and deviatoric stresses are higher in the lowlands than in the mountains. The quantitative analysis of the strain rate distribution and evolution, however, is out of scope of our study.

The values of τ_{xx} in the crust have been averaged within the region of the lowlands and the mountains, and the absolute magnitudes of these averages are plotted in Fig. 2 to compare the 2-D numerical results with the analytical results based on the thin sheet approximation. For the two-layer model (Fig. 2a), the analytical and numerical results agree better for larger viscosity ratios, R, between crust and mantle. For $R = 1000$, and lowlands and mountains of approximately equal width, the numerical results agree with the prediction of eq. (22). For $R = 1000$, an additional simulation to the one shown in Fig. 3(c), has been done with a viscosity of the crust of 10^{21} Pa·s and a viscosity of the mantle of 10^{18} Pa·s. The numerical results of these two simulations with $R = 1000$ provide similar deviatoric stress magnitudes showing that these magnitudes depend only on the viscosity ratio and not on the absolute values of
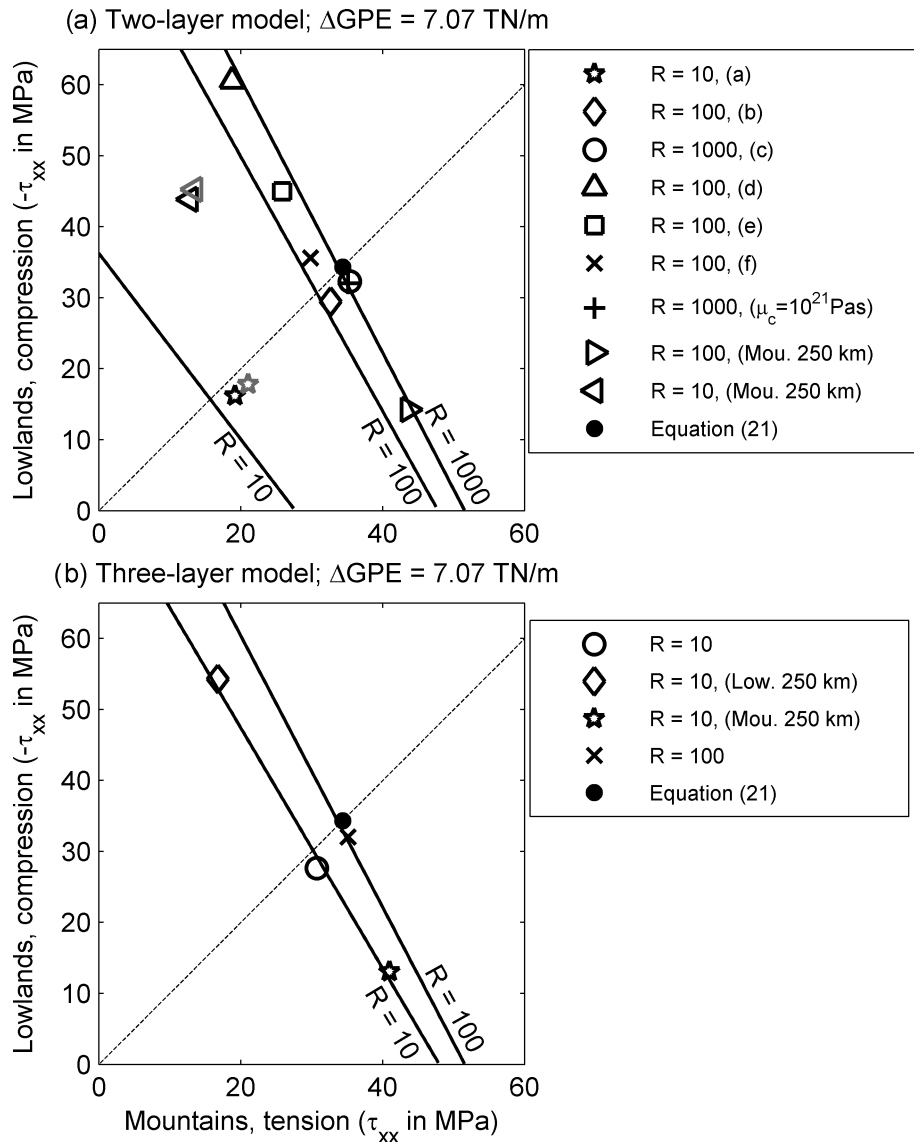
(a) Two-layer model; ΔGPE = 7.07 TN/m

(b) Three-layer model; ΔGPE = 7.07 TN/m

Figure 2. Absolute magnitudes of deviatoric stresses in the mountains versus the stress magnitudes in the lowlands for the two-layer (a) and three-layer (b) model. (a) The three solid black lines have been plotted with eq. (22) for three different viscosity ratios, *R*, and for the parameters displayed in Fig. 1(a). The symbols indicate averaged stress magnitudes from 2-D numerical simulations (see text and Fig. 3). Letters (a)–(d) in the legend refer to the corresponding simulations presented in Figs 3 and 4. The number (250 km) in the legend refers to simulations with a width of the mountains of 250 km and a width of the lowlands of 900 km. The grey star and triangle represent the values of the numerically calculated tectonic overpressure. All other values of tectonic overpressure have not been plotted because they are graphically indistinguishable from the values of the deviatoric stresses. (b) The two solid black lines have been plotted with eq. (22) for two different viscosity ratios, *R*, and for the parameters displayed in Fig. 1(b). The symbols indicate averaged stress magnitudes from 2-D three-layer simulations. The label (Low. 250 km) refers to a simulation with a width of the lowlands of 250 km, whereas the label (Mou. 250) refers to a simulation with a width of the mountains of 250 km.

viscosity, which is in agreement with eq. (22). For simulations shown in Figs 3(a)–(c), the deviatoric stress magnitudes in the mountains are a bit larger than the stress magnitudes in the lowlands because the lowlands are slightly wider (1000 km) than the mountains (900 km, Fig. 1). Two further simulations have been performed with the two-layer model for $R = 10$ and 100, and with a width of the mountains of only 250 km.

Additional simulations have been performed with the three-layer model to test the impact of a much less viscous asthenosphere below the lithosphere. Three simulations have been performed with $R = 10$ and different width of lowlands and mountains, and one simulation has been performed with $R = 100$ (Fig. 2b). For the three-layer

model, in contrast to two-layer models, the analytical and numerical results agree also for small viscosity ratios, $R = 10$, between crust and subcrustal lithosphere. The reason for this agreement is that the free-slip bottom boundary condition in the three-layer model is not applied at the bottom of the lithosphere, but at the bottom of the much less viscous asthenosphere, so that the stress state at the base of the lithosphere in the three-layer model is close to the compensation condition assumed for the thin sheet result of eq. (22).

The tectonic overpressure, P_O, is displayed in Fig. 4 for the 6 two-layer simulations displayed in Fig. 3 and for the initial geometry. The displayed tectonic overpressure has been calculated by
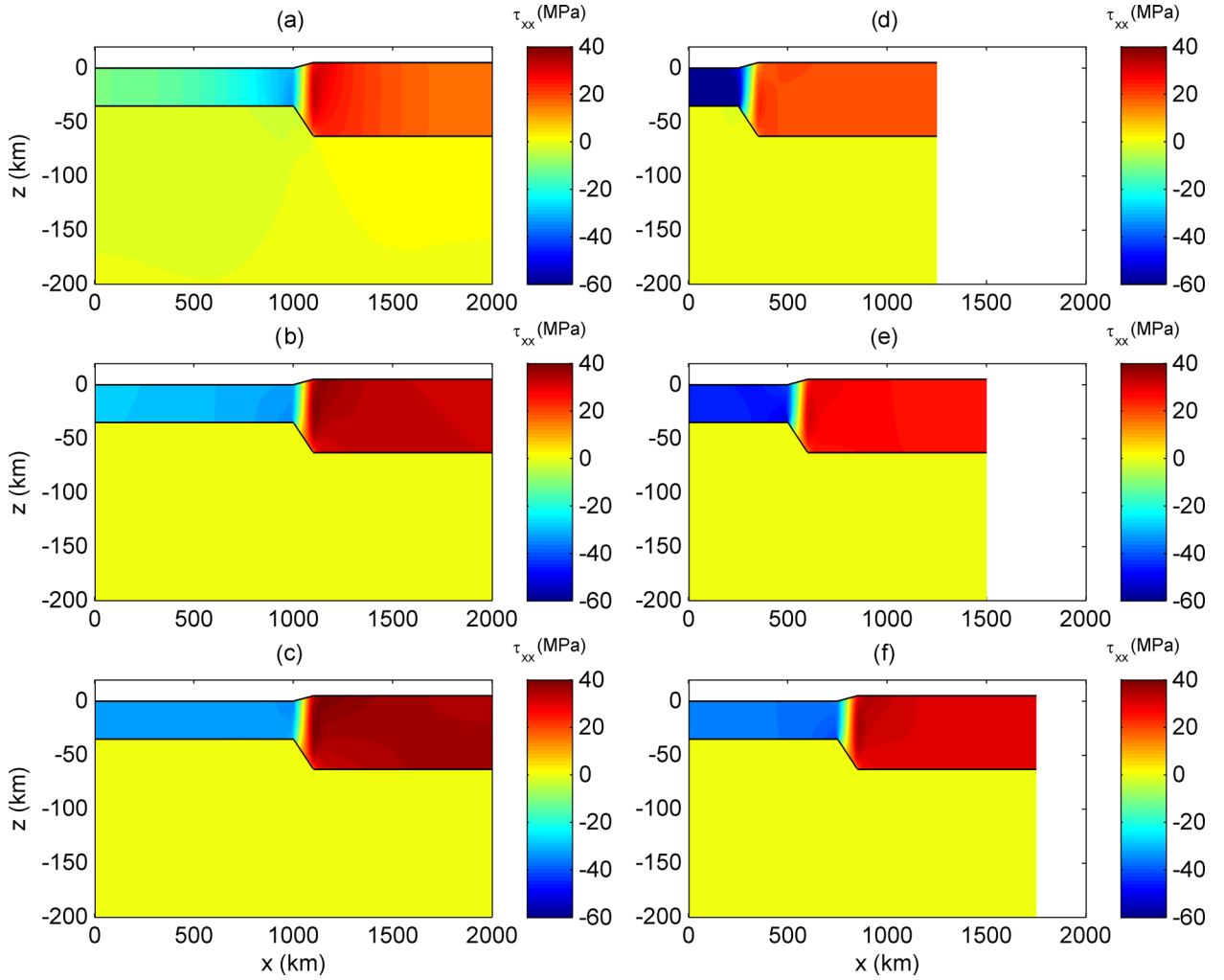
Figure 3. Colour plot of horizontal deviatoric stress, τ_{xx}, in MPa for six different two-layer model configurations for the initial geometry. (a) Viscosity of the crust is 10^{21} Pa·s and width of lowland is 1000 km. (b) Viscosity of the crust is 10^{22} Pa·s and width of lowland is 1000 km. (c) Viscosity of the crust is 10^{23} Pa·s and width of lowland is 1000 km. (d) Viscosity of the crust is 10^{22} Pa·s and width of lowland is 250 km. (e) Viscosity of the crust is 10^{22} Pa·s and width of lowland is 500 km. (f) Viscosity of the crust is 10^{22} Pa·s and width of lowland is 750 km. All other parameters are specified in Fig. 1(a). Results are only shown down to a depth of 200 km.

subtracting the lithostatic pressure, calculated from the modelled crustal geometry, from the pressure calculated with the numerical algorithm. The results show that absolute values of P_O are similar to the absolute values of τ_{xx} (Fig. 3) confirming the analytical relation $P_O = -\tau_{xx} + Q$ derived in the Appendix, and indicating that the impact of shear stresses, Q, is small for the considered model configuration (see also the Appendix). The values of P_O in the crust have also been averaged within the region of the lowlands and the mountains. Only the values of P_O for the simulation in Fig. 3(a) (with $R = 10$) are plotted in Fig. 2(a) (grey star) because all other values are graphically not distinguishable from the values of τ_{xx}, which indicates that the thin sheet approximation $P_O \approx -\tau_{xx}$ is valid for all two-layer simulations except the one with low viscosity ratio $R = 10$. For the three-layer simulations, the values of P_O have not been plotted in Fig. 2(b) because they are graphically not distinguishable from the values of τ_{xx}, which indicates that the thin sheet approximation $P_O \approx -\tau_{xx}$ is valid for all three-layer simulations; also for the ones with low viscosity ratio $R = 10$.

The horizontal force, ΔF_x, has been calculated for the initial geometry of the two-layer model using eq. (11) (Fig. 5). Furthermore,

the values of $\bar{\tau}_{xx}$ and $\bar{P}_O$ have been calculated from the numerical model results (Figs 3 and 4). For comparison, also the value of ΔGPE_{iso}, which assumes local isostasy (eq. 12) has been plotted. The values of ΔGPE_{iso} agree well with ΔF_x (Fig. 5). The numerical results further show that values of ΔF_x correspond to numerically calculated values of $\Delta\left(-\bar{P}_O + \bar{\tau}_{xx}\right)$ as predicted by the analytical results of the previous section. Values of $\Delta\bar{\tau}_{xx}$ do not correspond directly to values of ΔGPE_{iso} or ΔF_x and are about a factor of two smaller than those predicted by the analytical results of the previous section (eq. 9).

A two-layer and a three-layer simulation with $R = 10$ have been performed until a (arbitrary) time of 245 kyr to investigate the evolution of stress and pressure in the crust during progressive equilibrating flow that is caused by the lateral variation in *GPE* (Fig. 6). The evolution of the horizontal profiles of ΔGPE_{iso}, ΔF_x, $\bar{\tau}_{xx}$ and $\bar{P}_O$ has been calculated for the two-layer (Figs 6a–c) and the three-layer (Figs 6d–f) model. For the initial geometry (at time 0 kyr), the profiles of ΔGPE_{iso} and ΔF_x agree for both the two-layer (Fig. 6a) and the three-layer (Fig. 6d) model. After 120 kyr, the values of ΔGPE_{iso} and ΔF_x differ strongly for the two-layer model, especially around the region with the topographic variation
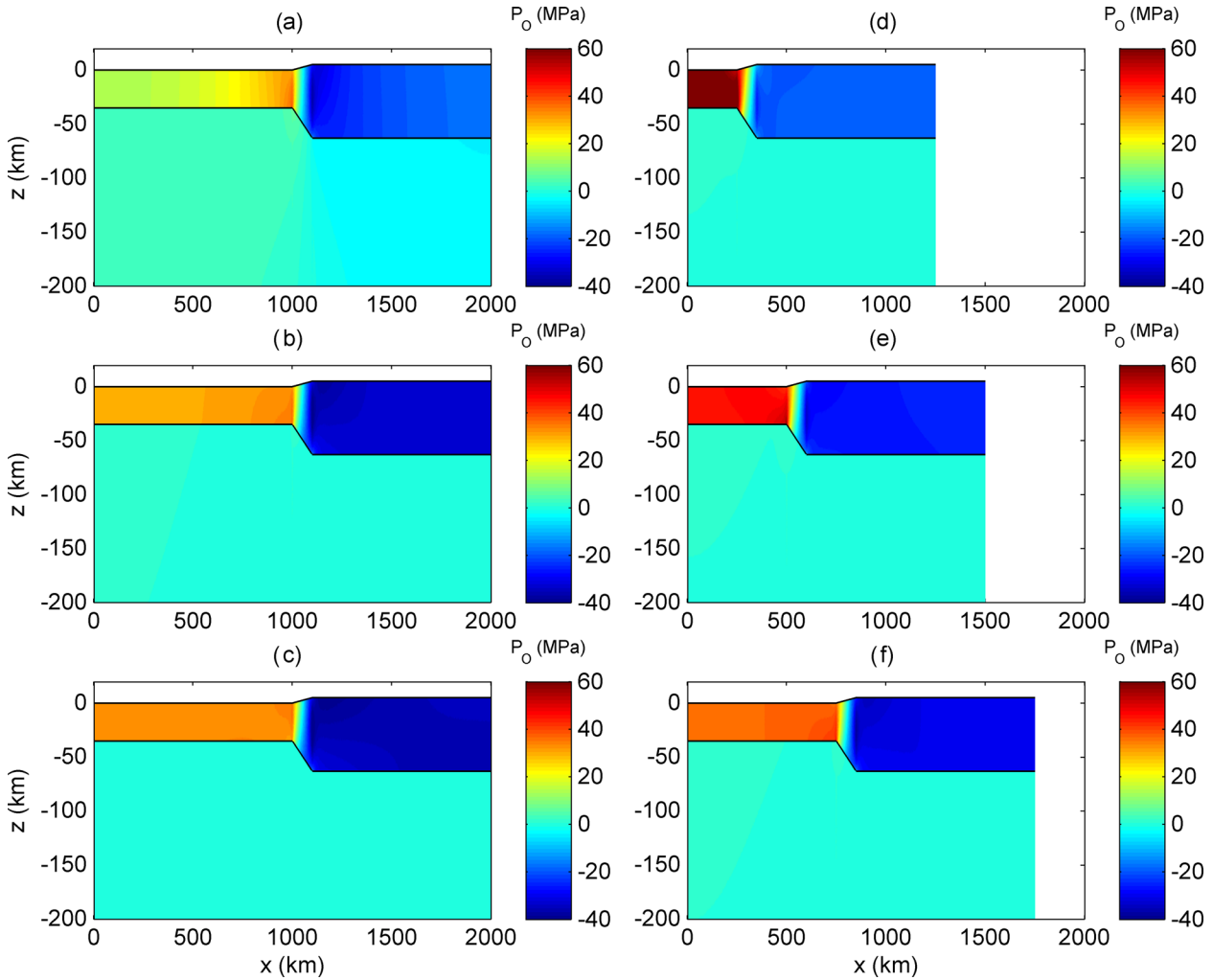
Figure 4. Colour plot of tectonic overpressure, P_O, in MPa for six different two-layer model configurations for the initial geometry. (a) Viscosity of the crust is 10^{21} Pa·s and width of lowland is 1000 km. (b) Viscosity of the crust is 10^{22} Pa·s and width of lowland is 1000 km. (c) Viscosity of the crust is 10^{23} Pa·s and width of lowland is 1000 km. (d) Viscosity of the crust is 10^{22} Pa·s and width of lowland is 250 km. (e) Viscosity of the crust is 10^{22} Pa·s and width of lowland is 500 km. (f) Viscosity of the crust is 10^{22} Pa·s and width of lowland is 750 km. All other parameters are specified in Fig. 1(a). Results are only shown down to a depth of 200 km.

(Fig. 6b). Numerical values of $\Delta\left(-\bar{P}_O + \bar{\tau}_{xx}\right)$ agree with values of ΔF_x. The difference between values of ΔGPE_{iso} and ΔF_x indicates that the corresponding numerically calculated crustal geometries, that is, elevation and root, do not correspond to isostatic conditions. This deviation from isostasy in the two-layer model is caused by non-negligible shear stresses in the crust and mantle caused by the equilibrating flow, especially in the region around the topographic variation. For the three-layer model, the values of ΔGPE_{iso} and ΔF_x are similar after 120 kyr (Fig. 6e) indicating that the crustal elevation and root are in isostatic equilibrium. The crustal geometry of the mountains in the three-layer model is in isostatic equilibrium during the deformation because the weak asthenosphere below the lithosphere enables that the compensation condition can be fulfilled at the base of the lithosphere below the mountains. After 245 kyr, the values of ΔGPE_{iso} and ΔF_x have further decreased in the two-layer (Fig. 6c) and the three-layer (Fig. 6e) models. Values of ΔGPE_{iso} and ΔF_x still differ significantly in the two-layer model, whereas values of ΔGPE_{iso} and ΔF_x agree in the three-layer model. For all times and for both the two-layer and the three-layer models, eq. (11) correctly predicts the values of $\Delta F_x = \Delta\left(-\bar{P}_O + \bar{\tau}_{xx}\right)$ resulting from the numerical simulation.

For completeness, also a three-layer simulation has been performed with a viscosity of the crust of 10^{22} Pa·s and a larger viscosity of the lithospheric mantle of 10^{23} Pa·s, which represents an entirely strong lithosphere overlying a much less viscous asthenosphere (10^{17} Pa·s). The horizontal profiles of the depth-integrated values for two arbitrary times (4 and 8.1 Myr; the times are larger than in Fig. 6 because for the much stronger lithospheric mantle it takes much more time to have a significant deformation) show that around the topographic variation between lowlands and mountains the crustal geometry does not correspond to isostatic equilibrium (Fig. 7). This deviation from isostasy can be explained with significant shear stresses around the crust–mantle boundary and significant stresses within the strong lithospheric mantle. Despite the significant deviations from isostasy, the analytical prediction of ΔF_x from eq. (11) agrees with the numerical results.

DISCUSSION

The results presented here show that $\bar{P}_O \approx -\bar{\tau}_{xx}$ and that $\Delta\left(-\bar{P}_O + \bar{\tau}_{xx}\right) = \Delta F_x$ for the considered model configuration. A similar model configuration was applied by Molnar & Lyon-Caen
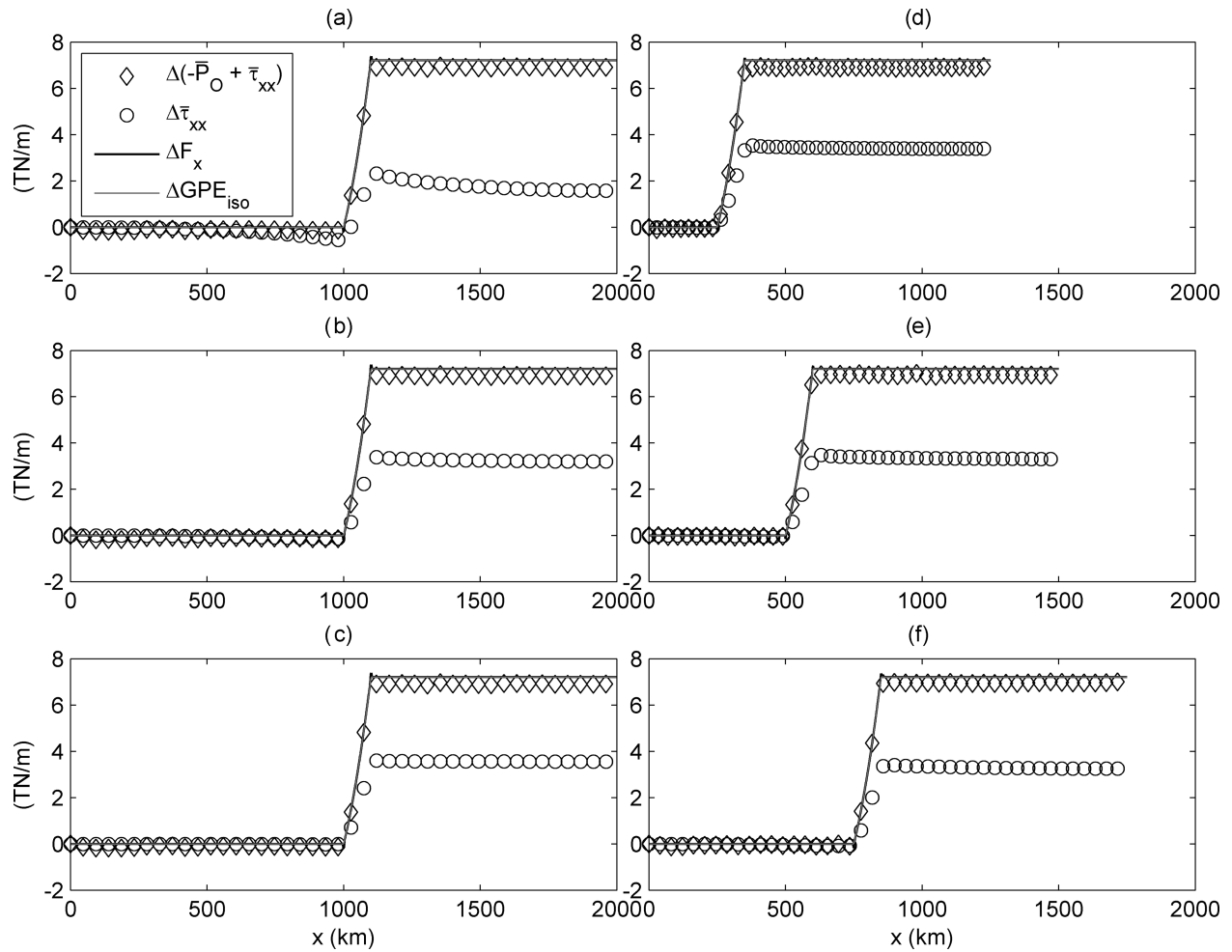
Figure 5. Results for the two-layer models for the initial geometry. Horizontal profiles of differences in the depth-integrated sum of tectonic overpressure and horizontal deviatoric stress, $\Delta\left(-\bar{P}_O + \bar{\tau}_{xx}\right)$ (calculated from 2-D numerical results), differences in depth-integrated horizontal deviatoric stress, $\Delta\bar{\tau}_{xx}$ (calculated from 2-D numerical results), differences in the horizontal force per unit length, ΔF_x (calculated analytically from eq. 11) and in GPE, $\Delta GPE_{\mathrm{iso}}$ (calculated analytically from eq. 12; result is based on assumption of local isostasy). The six subplots (a)–(f) correspond to the same simulations as presented in Figs 3 and 4.

(1988), and they estimated that ΔF_x is approximately 7 TN m^{-1} for Tibet. Therefore, absolute magnitudes of $\bar{P}_O$ and $\bar{\tau}_{xx}$ are approximately 3.5 TN m^{-1} each. These estimates for $\bar{\tau}_{xx}$ agree with estimates presented by Ghosh *et al.* (2006, 2009, 2013). The results show that the existence of the Tibetan Plateau is evidence for tectonic overpressure that is of the same magnitude than the deviatoric stress. Both tectonic overpressure and deviatoric stresses are necessary to build and support high continental plateaus, such as present in Tibet and the Andes. The magnitudes of $\bar{\tau}_{xx}$ estimated from *GPE* variations can be considered as minimum estimates of $\bar{\tau}_{xx}$ during plateau formation because $\bar{\tau}_{xx}$ resulting from *GPE* represent stresses necessary to support a static, isostatically compensated thickened crust (e.g. England & Houseman 1986). England & Houseman (1986) calculated values of vertically integrated stress differences of 20 (±5) TN m^{-1} with a thin viscous sheet model applied to the formation of the Tibetan Plateau which are significantly larger than estimated from *GPE* variations between Tibet and surrounding lowlands. They argue that such values reflect the stresses required to drive the deformation of the viscous sheet. In another study considering convective thinning of the lithosphere, England & Houseman (1989) showed that viscous stresses resulting from the deformation amount to 1–4 TN m^{-1}. These studies show that stress estimates

resulting from *GPE* data are minimum (static) stress estimates and suggest that stresses in nature are usually larger due to the additional (dynamic) tectonic deformations. Therefore, absolute magnitudes of $\bar{\tau}_{xx}$ and $\bar{P}_O$ could have been larger than 3.5 TN m^{-1} during the formation of the Tibetan Plateau.

In several studies, Ghosh and coauthors (e.g. Ghosh *et al.* 2006, 2009, 2013) have argued that Molnar and coauthors (e.g. Molnar & Lyon-Caen 1988; Molnar *et al.* 1993) have overestimated depth integrals or depth averages of deviatoric stress magnitudes in Tibet by approximately a factor of two. Our results show that such overestimation actually does not exist because Ghosh and coauthors estimate magnitudes of $\bar{\tau}_{xx}$, the depth-integrated value of the deviatoric stresses, while Molnar and coauthors estimate magnitudes of $F_x = -\bar{P}_O + \bar{\tau}_{xx}$, the driving force per unit length caused by *GPE* variations. Our results show that if vertical integrals of shear stresses are small then $\bar{P}_O \approx -\bar{\tau}_{xx}$ and, hence, Molnar and coauthors estimate magnitudes of $F_x = 2\bar{\tau}_{xx}$. Therefore, the factor two difference between estimates of Molnar and coauthors and Ghosh and coauthors is not due to a 2-D approximation or inappropriate definition of deviatoric stress, as stated by Ghosh *et al.* (2006), but due to a comparison of different quantities, that is, F_x with $\bar{\tau}_{xx}$. The recent development of stress estimations using thin viscous sheet
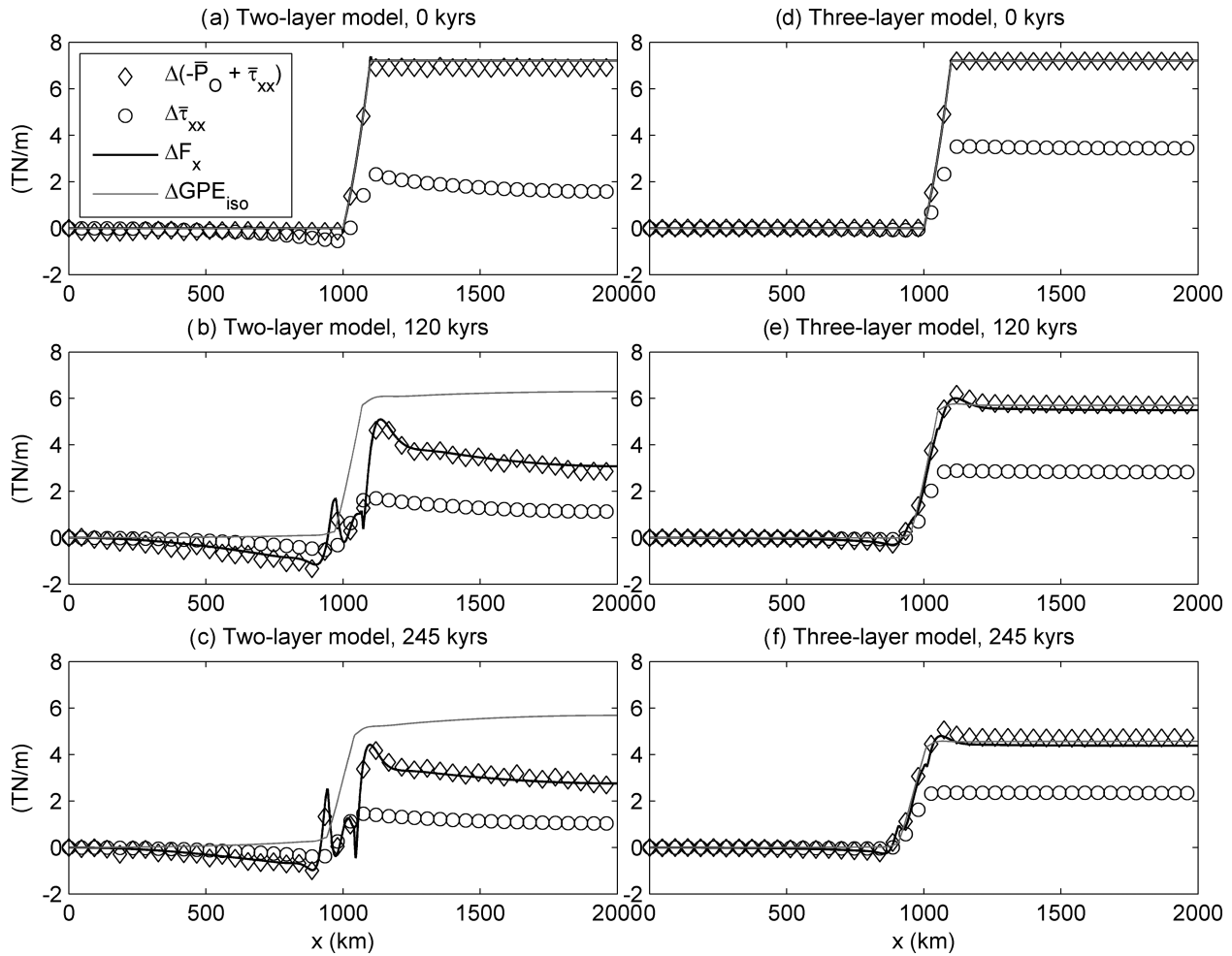
Figure 6. Results for the two-layer model, (a)–(c), and for the three-layer model, (d)–(f), for a viscosity ratio of $R = 10$ for different stages (times) of deformation. Horizontal profiles of differences in the depth-integrated sum of tectonic overpressure and horizontal deviatoric stress, $\Delta\left(-\bar{P}_O + \bar{\tau}_{xx}\right)$ (calculated from 2-D numerical results), differences in depth-integrated horizontal deviatoric stress, $\Delta\bar{\tau}_{xx}$ (calculated from 2-D numerical results), differences in the horizontal force per unit length, ΔF_x (see eq. 11) and in *GPE*, ΔGPE_{iso} (see eq. 12; result is based on assumption of local isostasy). Subplots (a) and (d) show results for 0 kyr (initial geometry), subplots (b) and (e) for 120 kyr and (c) and (f) for 245 kyr.

models in Ghosh *et al.* (2013), which shows that the integrated deviatoric stress in sum with the basal drag at the lithosphere is equal to estimates of Molnar & Lyon-Caen (1988), means only that the estimated basal drag is of the same magnitude as the integrated deviatoric stress. However, if the magnitude of the basal drag is of the same order as the magnitude of the deviatoric stresses in the sheet, then the contributions of the shear stresses, that is, $Q(x, Sb)$ and $\bar{Q}(x)$, may not be negligible in the depth-integrated force balance equations and the applied thin sheet approximation may be considerably inaccurate.

The stresses resulting from the lateral variation in *GPE* related to the Tibetan Plateau could have potentially caused folding (buckling) of the Indo-Australian Plate south of India (Molnar *et al.* 1993). Martinod & Molnar (1995) calculated analytically that a depth integrated difference between horizontal and vertical stresses of approximately 4.8 TN m^{-1} could fold the Indian oceanic lithosphere. Under the thin sheet approximation of negligible shear stresses σ_{xz} throughout the lithosphere, the total vertical stress is equal to the lithostatic pressure, or 'static stress' (due to vertical force balance), and hence the depth-integrated difference between horizontal and vertical stresses is identical to the depth-integrated difference between the horizontal stress and the lithostatic pressure (i.e. the hor-

izontal driving force per unit length). Consequently, the magnitude of the horizontal driving force per unit length of approximately 7 TN m^{-1} resulting from the *GPE* variation related to the Tibetan Plateau is sufficient to fold the lithosphere. In contrast, Ghosh *et al.* (2006) argued that the Tibetan Plateau causes depth-integrated deviatoric stresses that are smaller than 4.8 TN m^{-1} (here approximately 3.5 TN m^{-1}), and that hence the uplift of the Tibetan Plateau is unlikely the single factor for the onset of folding in the Indian Ocean. However, the horizontal force per unit length that causes folding is calculated with the deviation of the total horizontal stresses from the lithostatic pressure that is equal to the vertical total stress in the 'traditional' thin sheet approximation, and hence includes contributions from both deviatoric stresses and overpressure (e.g. Biot 1961). Therefore, the correct magnitude to estimate whether the uplift of the Tibetan Plateau could have caused folding is 7 TN m^{-1}, because this value includes the contributions of the overpressure (i.e. $F_x = -\bar{P}_O + \bar{\tau}_{xx} = \bar{\sigma}_{xx} - \bar{\sigma}_{xx}^s$, see eq. 7).

Our analytical predictions compare well with results of the two-layer numerical simulations, although the accuracy of the analytical prediction for low $R = 10$ may be questioned (Fig. 2). This misfit is caused by the deviation from the compensation condition at the base of the models with low R. The bottom compensation condition
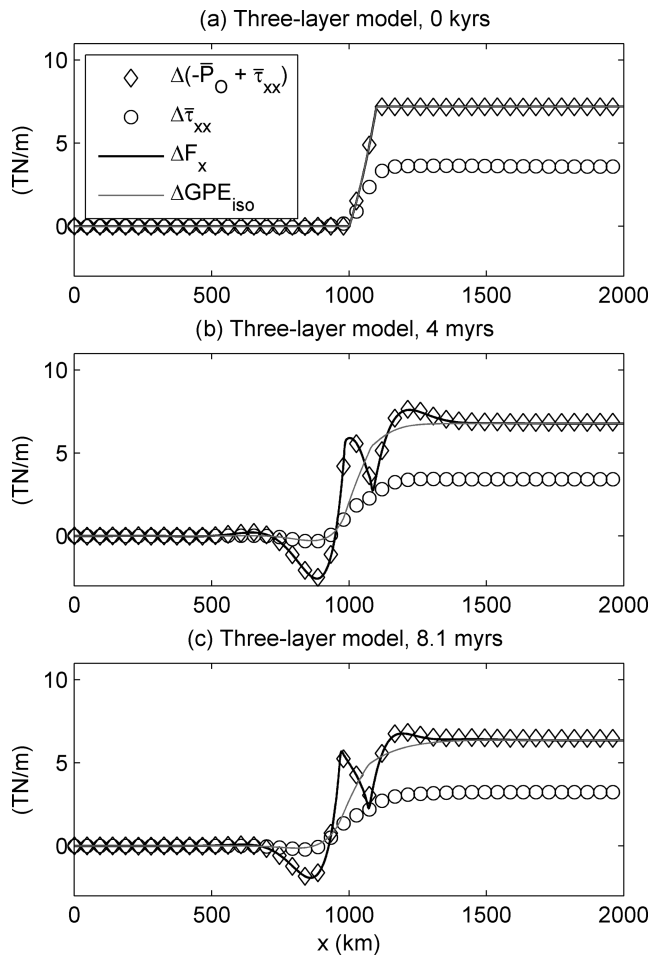
Figure 7. Results for the three-layer model for a viscosity of the crust of 10^{22} Pa·s, a viscosity of the lithospheric mantle of 10^{23} Pa·s and a viscosity of the asthenosphere of 10^{17} Pa·s, for different stages (times) of deformation. Horizontal profiles of differences in the depth-integrated sum of tectonic overpressure and horizontal deviatoric stress, $\Delta\left(-\bar{P}_O + \bar{\tau}_{xx}\right)$ (calculated from 2-D numerical results), differences in depth-integrated horizontal deviatoric stress, $\Delta\bar{\tau}_{xx}$ (calculated from 2-D numerical results), differences in the horizontal force per unit length, ΔF_x (see eq. 11) and in *GPE*, ΔGPE_{iso} (see eq. 12; result is based on assumption of local isostasy).

assumes that the material at the base is much weaker (i.e. has much lower viscosity) than the average over the thin sheet. In the examples of our two-layer study, the upper layer should be much stronger than the bottom layer to approach the compensation condition along the base ($R \gg 1$). Whereas a low R does not cause errors in the numerical models, as they do not utilize the compensation condition explicitly, the thin sheet approach is based on the condition of compensation, and hence thin sheet models are more accurate for higher values of R in the two-layer model. The thin sheet predictions compare well with numerical results even for low values of R if a three-layer numerical model is applied in which the model lithosphere overlies a much less viscous asthenosphere. The results of two series of numerical simulations indicate that the distribution of stresses within strong layers of the lithosphere is controlled by R, and that the accuracy of analytical predictions based on the thin sheet approximation is controlled by the viscosity ratio between the top and bottom layer in the numerical model. The high viscosity ratio between the top layer (crust) and the bottom layer (the lithospheric mantle in the two-layer model and the asthenosphere in the three-layer model)

facilitates the condition of compensation at the base of the model. Consequently, thin sheet results are more accurate for models with a strong rheological stratification.

The assumption that the pressure is equal to the lithostatic pressure during the formation of continental plateaus is in fundamental contrast to the mechanical concept of force balance. More generally, our results show that this assumption is not applicable if there are lateral variations in *GPE*. *GPE* variations may likely occur during mountain building, subduction and continental collision. However, the assumption of a lithostatic pressure is frequently applied for the reconstruction of the tectonic evolution of mountain ranges and continental plateaus, especially when such reconstructions are based on P-T paths obtained from mineral assemblages. The results presented here provide strong arguments that tectonic overpressures of tens of MPa (as vertical average) exist during mountain building, and these results are independent on the actual strength or rheology of the involved rocks. Our simulations show magnitudes of tectonic overpressure up to 60 MPa (Fig. 4d). In our simulations, the tectonic overpressure is more or less constant with depth in the crust due to the applied homogeneous viscosity. However, yield strength envelopes for the lithosphere show that in nature the magnitudes of deviatoric stress can vary significantly with depth due to variations of material properties and the related flow laws (e.g. Kohlstedt *et al.* 1995; Burov 2010). Therefore, in certain depth levels the magnitudes of tectonic overpressure and deviatoric stress can be significantly larger than the average magnitude of 60 MPa, because these magnitudes can be significantly smaller in other depth levels, but the depth-integrated values are unchanged and controlled by the *GPE* variation. Lechmann *et al.* (2014) applied a full 3-D finite element model with vertically varying viscosities (hence, vertically varying strength) to the modern India–Asia collisional system, and showed that the maximal tectonic overpressure in a strong Indian lower crust can be approximately 500 MPa even if there is no far-field deformation or stress applied. Several studies have quantified possible maximal magnitudes of tectonic overpressure for a variety of geodynamic scenarios and these magnitudes are typically on the order of 1 GPa corresponding to a depth of about 36 km if a lithostatic pressure and a density of 2800 kg m^{-3} is assumed (e.g. Mancktelow 1995; Petrini & Podladchikov 2000; Schmalholz & Podladchikov 2013). These studies also show that the maximum tectonic overpressure is usually of the order of the maximum deviatoric stress in a homogeneous crust, which generally agrees with our results for the approximate equality of depth-integrated tectonic overpressure and deviatoric stress. In contrast to these studies suggesting significant deviatoric stresses, there exist a number of studies arguing for negligible deviatoric stresses (or strength) within the lithosphere. Arguments are often based on observations, such as the common appearance of tensile veins or the presence of clay-like minerals and fluids in crustal rocks, and these observations are used to infer negligible strength of crustal rocks undergoing metamorphism across all metamorphic grades and at all lithospheric depths (e.g. Brace *et al.* 1970; Etheridge 1983; Sibson 1990; Schreyer 1995). The acceptance of negligible rock strength at any lithospheric depth (i.e. $< \sim 20$ MPa; Etheridge 1983) often leads to further assumptions of similarly negligible deviations of the stress components and the thermodynamic pressure from the lithostatic pressure. However, this possibility is firmly ruled out by magnitudes of lateral *GPE* variations, such as approximately 7 TN m^{-1} in Tibet. This magnitude of *GPE* variation requires a deviation of the horizontal stress from the lithostatic stress of 70 MPa in average across the entire lithosphere (assuming 100 km thickness; Molnar & Lyon-Caen 1988). Assuming further that the colder and stronger parts of the lithosphere, that

are responsible for its 'effective elastic thickness', all together take up not more than say one-third of the total lithospheric thickness, then this strong part of the lithosphere must sustain non-lithostatic stress anomalies of approximately 200 MPa in order to maintain the average stress deviation from the lithostatic pressure of 70 MPa. The physical relation between the average non-lithostatic stress anomaly and the *GPE* variations can, therefore, be applied to falsify statements that crustal rocks may not sustain significant deviations (say >10 MPa) from the lithostatic pressure over geological timescales at any depth of the lithosphere. In contrast, the *GPE*-based argument concerning stress magnitudes is known since the classical work of Jeffrey (1959) and is recognized as robust estimate for stress magnitudes due to its rheology independence (e.g. Kanamori 1980). The relation between the *GPE* and the sum of two depth-integrated quantities, deviatoric stress (or strength) and overpressure, requires that at least one of the two quantities must be significant at some depth level. Recent numerical simulations showed that for a 'weak' scenario, that is, if rocks lost their strength by some strain-weakening mechanism within a crustal-scale shear zone, the weak rheology sets a limit, as expected, only for the value of the deviatoric stresses but not for the overpressure (Schmalholz & Podladchikov 2013). Consequently, for such 'weak' scenario, the non-lithostatic pressure anomaly must be the reason for the significant deviation of the total horizontal stress from the lithostatic pressure, because the total horizontal stress would only 'weakly' deviate from the actual dynamic pressure and the other stress components.

Values of $\Delta GPE_{\mathrm{iso}}$ deviate the more from ΔF_x the more the crust is deformed for low values of R during the equilibrating flow of the two-layer model that eventually generates a crust of constant thickness (Fig. 6). This deviation shows that the topography and the corresponding root do not follow the isostatic relation. The reason for the non-isostatic condition is that viscous stresses in the deforming mantle contribute to the support of crust and surface elevations, and that a free-slip boundary condition is applied at the model bottom. However, the numerical results show that eq. (11) for ΔF_x can be used even for the free-slip condition and the non-isostatic crustal geometry applied at the model bottom in our numerical simulation to estimate magnitudes of $-\bar{P}_O + \bar{\tau}_{xx}$. Therefore, eq. (11)

is useful to estimate values of $-\bar{P}_O + \bar{\tau}_{xx}$ because it is not based on the assumption of local isostasy, which may not always be satisfied in nature. The simulation of Fig. 4(a) has been run also with a viscosity of the mantle of 10^{18} Pa·s (see also Fig. 2) and for this significantly smaller mantle viscosity (and hence larger R) the profiles of $\Delta GPE_{\mathrm{iso}}$ and ΔF_x agree well showing that the numerically calculated crustal geometry corresponds to the isostatic condition. Deviations are only observed around the transition between lowlands and mountains.

Our results are also applicable to 3-D plateaus assuming a similar shape of the crust in the third dimension and assuming that magnitudes of $\bar{\tau}_{yy}$ (with y being the horizontal coordinate orthogonal to the horizontal x-direction) are significantly smaller than magnitudes of $\bar{\tau}_{xx}$. For more complicated 3-D geometries, for example, around the corners of plateaus, the exact magnitudes of the stresses and tectonic overpressure have to be calculated with thin viscous sheet or full 3-D models (e.g. Lechmann *et al.* 2011).

CONCLUSIONS

We rederived and analysed the integrated balance of stresses for large-scale lithospheric deformations, and clarified the assumptions used in the derivations. We showed that if the constant base of the integration is free from shear stresses and the upper surface is stress-free, then the derived integrated balance of stresses is valid even for fair variations of topography. In particular, we showed that lateral variations in *GPE* are equal to variations in the sum of the depth-integrated tectonic overpressure and the depth-integrated horizontal deviatoric stress (Table 2). We also showed that, despite previously published derivations, this equality holds for non-isostatic conditions and non-negligible shear stresses. If the depth-integrated shear stresses are constant in the horizontal direction then lateral variations in *GPE* are equal to twice the variations of depth-integrated horizontal deviatoric stress (Table 2).

Tectonic overpressure can exist at the compensation depth even if all the deviatoric stresses are zero there because the tectonic overpressure is related to horizontal gradients of the shear stresses

Table 2. Summary of main results and the related assumptions.

Description	Assumptions	Main resulting equations
No shear stress at the model base, *Sb*.	$\tau_{xz}(x, Sb) = 0$	$\Delta F_x = \Delta\left(-\bar{P}_O + \bar{\tau}_{xx}\right) = \Delta(GPE)$
No shear stress at base and constant integrated shear stress.	$\tau_{xz}(x, Sb) = \frac{\partial}{\partial x}\bar{Q} = 0$	$2\Delta\bar{\tau}_{xx} = \Delta(GPE)$
Zero deviatoric stresses at the model base.	$\tau_{xz}(x, Sb) = \tau_{zz}(x, Sb) = 0$	$P_O(x, Sb) = Q(x, Sb)$
Compensation: Zero deviatoric stresses in a layer at the base.	$\tau_{xz}(x, Sb) = \tau_{zz}(x, Sb) = \frac{\partial \tau_{xz}}{\partial z}(x, Sb) = 0$	$\Delta\sigma_{zz}(x, Sb) = 0$
Local isostasy: Zero deviatoric stresses in a basal layer and constant integrated shear stress.	$\tau_{xz}(x, Sb) = \tau_{zz}(x, Sb) = \frac{\partial \tau_{xz}}{\partial z}(x, Sb) = \frac{\partial \bar{Q}}{\partial x}(x, Sb) = 0$	$\Delta P_L(Sb) = 0$
'Traditional' thin sheet model: Zero shear stress, τ_{xz}, everywhere.	$\tau_{xz}(x, z) = 0$	$2\Delta\bar{\tau}_{xx} = \Delta(GPE)$ $\Delta P_L(Sb) = 0$ $P_O(x, Sb) = 0$ $P_O = -\tau_{xx}$

integrated over the entire depth of the lithosphere (Table 2). The vertical total stress is constant along the compensation depth if there is an inviscid layer at the compensation depth (Table 2). Local isostasy means that the lithostatic pressure is constant along the compensation depth, and exists if there is an inviscid layer at the compensation depth and if additionally the depth-integrated shear stresses are constant (Table 2).

The traditional derivation of the thin sheet model is based on the strong assumption that the shear stresses σ_{xz} are zero everywhere within the lithosphere, and, therefore, in the thin sheet model the variations in *GPE* are equal to twice the variations of the depth-integrated horizontal deviatoric stress (Table 2). We rederived here equations based on the thin sheet approximation and showed that the assumption of the traditional derivation (i.e. zero shear stress σ_{xz} everywhere) is unnecessarily strong. The governing equations of the thin sheet approximation are valid even for non-zero vertical shear stress σ_{xz} as soon as the integrated measure of the shear stresses, $Q(x, z)$, has the following properties: its value at the base, $Q(x, Sb)$, and its depth integral, $\bar{Q}(x)$, are nearly constants within the model domain. Furthermore, for 2-D configurations with an integrated measure of the shear stresses, $Q(x, z) = 0$, the tectonic overpressure has the same absolute magnitude as the deviatoric stress.

The thin sheet approximation assumes two mechanical conditions simultaneously, namely, a finite average strength of the sheet and the compensation (i.e. zero strength) at the base of the sheet. These two conditions imply a strong rheological stratification of the sheet and, consequently, of the modelled lithosphere. We argue that this approximation is more accurate for stronger rheological variations with depth. Our numerical simulations show that the thin sheet approximation is accurate for a lithosphere consisting of a mechanically strong top layer (here the crust) and a mechanically weaker bottom layer (here either the mantle in the two-layer model or the asthenosphere in the three-layer model). For a viscosity ratio between top and bottom layer of 10^3–10^7, the thin sheet approximation is accurate, whereas for a viscosity ratio of 100 and smaller it is not.

An inviscid layer below the compensation depth guarantees the compensation condition, namely, negligible deviatoric stresses, and therefore a constant pressure and vertical total stress along the compensation depth. This compensation condition, however, does not guarantee a constant lithostatic pressure at the compensation depth and thus, the condition of local isostasy. The equality of pressure and lithostatic pressure is possible only if the horizontal gradients of the shear stresses integrated vertically throughout the entire lithosphere are zero. We derived an equation (eq. 13) that quantifies the variations of the lithostatic pressure along the compensation depth as function of the shear stress distribution above the compensation depth.

Lateral variations in *GPE* such as observed around high continental plateaus in Tibet and the Andes must cause tectonic overpressure. Both, tectonic overpressure and deviatoric stress, which are approximately equal in magnitude, are required to build and support continental plateaus. Therefore, the existence of high continental plateaus is a proof for the existence of tectonic overpressure in the continental lithosphere. Such overpressures are independent of rock rheology, flow law or rock strength. For Tibet, the depth-integrated tectonic overpressure required to statically support the Tibetan Plateau has a magnitude of approximately 3.5 TN m^{-1}, which corresponds to a typical value of the force per unit length caused by ridge push. During active tectonic deformation of continents the magnitudes of tectonic overpressure and deviatoric stress are likely even larger as the magnitudes necessary to support a static

continental plateau. Deviatoric stresses and tectonic overpressure can vary significantly with depth in the lithosphere. Consequently, the *a priori* assumption of a lithostatic pressure everywhere within the lithosphere during mountain building and plateau formation is not justified, and is likely considerably inaccurate.

The magnitude of the horizontal driving force per unit length, that is, the depth-integrated deviation of the horizontal total stress from the lithostatic pressure (or static stress), of approximately 7 TN m^{-1} resulting from the *GPE* variation related to the Tibetan Plateau is sufficient to fold the Indian oceanic lithosphere.

REFERENCES

Artyushkov, E., 1973. Stresses in lithosphere caused by crustal thickness inhomogeneities, *J. geophys. Res.,* **78,** 7675–7708.

Biot, M.A., 1961. Theory of folding of stratified viscoelastic media and its implications in tectonics and orogenesis, *Bull. geol. Soc. Am.,* **72,** 1595–1620.

Bird, P. & Piper, K., 1980. Plane-stress finite-element models of tectonic flow in Southern-California, *Phys. Earth planet. Inter.,* **21,** 158–175.

Brace, W.F., Ernst, W.G. & Kallberg, R.W., 1970. An experimental study of tectonic overpressure in Franciscan rocks, *Bull. geol. Soc. Am.,* **81,** 1325–1338.

Bronstein, I.N., Semendjajew, K.A., Musiol, G. & Mühlig, H., 1997. *Taschenbuch der Mathematik*, 3rd edn, Verlag Harri Deutsch, Thun, Frankfurt am Main.

Burov, E.B., 2010. The equivalent elastic thickness (T-e), seismicity and the long-term rheology of continental lithosphere: time to burn-out "creme brulee"? Insights from large-scale geodynamic modeling, *Tectonophysics,* **484,** 4–26.

Dabrowski, M., Krotkiewski, M. & Schmid, D.W., 2008. MILAMIN: MATLAB-based finite element method solver for large problems, *Geochem. Geophys. Geosyst.,* **9,** QO4030, doi:10.1029/2007GC001719.

Dalmayrac, B. & Molnar, P., 1981. Parallel thrust and normal faulting in Peru and constraints on the state of stress, *Earth planet. Sci. Lett.,* **55,** 473–481.

England, P. & Houseman, G., 1986. Finite strain calculations of continental deformation .2. Comparison with the India-Asia collision zone, *J. geophys. Res.-Solid Earth Planets,* **91,** 3664–3676.

England, P. & Houseman, G., 1989. Extension during continental convergence, with application to the Tibetan plateau, *J. geophys. Res.-Solid Earth Planets,* **94,** 17 561–17 579.

England, P. & McKenzie, D., 1982. A thin viscous sheet model for continental deformation, *Geophys. J. R. astr. Soc.,* **70,** 295–321.

England, P. & McKenzie, D., 1983. Correction to—a thin viscous sheet model for continental deformation, *Geophys. J. R. astr. Soc.,* **73,** 523–532.

England, P. & Molnar, P., 1997. Active deformation of Asia: from kinematics to dynamics, *Science,* **278,** 647–650.

Ernst, W.G., 2001. Subduction, ultrahigh-pressure metamorphism, and regurgitation of buoyant crustal slices—implications for arcs and continental growth, *Phys. Earth planet. Inter.,* **127,** 253–275.

Etheridge, M.A., 1983. Differential stress magnitudes during regional deformation and metamorphism—upper bound imposed by tensile fracturing, *Geology,* **11,** 231–234.

Flesch, L.M., Haines, A.J. & Holt, W.E., 2001. Dynamics of the India-Eurasia collision zone, *J. geophys. Res.,* **106,** 16 435–16 460.

Ghosh, A., Holt, W.E., Flesch, L.M. & Haines, A.J., 2006. Gravitational potential energy of the Tibetan Plateau and the forces driving the Indian plate, *Geology,* **34,** 321–324.

Ghosh, A., Holt, W.E. & Flesch, L.M., 2009. Contribution of gravitational potential energy differences to the global stress field, *Geophys. J. Int.,* **179,** 787–812.

Ghosh, A., Holt, W.E. & Wen, L.M., 2013. Predicting the lithospheric stress field and plate motions by joint modeling of lithosphere and mantle dynamics, *J. geophys. Res.-Solid Earth,* **118,** 346–368.

Houseman, G. & England, P., 1986. Finite strain calculations of continental deformation. 1. Method and general results for convergent zones, *J. geophys. Res.,* **91,** 3651–3663.

Jeffrey, H., 1959. *The Earth*, Cambridge University press.

Jolivet, L., Faccenna, C., Goffe, B., Burov, E. & Agard, P., 2003. Subduction tectonics and exhumation of high-pressure metamorphic rocks in the Mediterranean orogens, *Am. J. Sci.,* **303,** 353–409.

Jones, C.H., Unruh, J.R. & Sonder, L.J., 1996. The role of gravitational potential energy in active deformation in the southwestern United States, *Nature,* **381,** 37–41.

Kanamori, H., 1980. The state of stress in the Earth's lithosphere, in *Physics of the Earth's Interior*, pp. 531–554, eds Dziewonski, A. & Boschi, E., North-Holland.

Kohlstedt, D.L., Evans, B. & Mackwell, S.J., 1995. Strength of the lithosphere—constraints imposed by laboratory experiments, *J. geophys. Res.-Solid Earth,* **100,** 17 587–17 602.

Lechmann, S.M., May, D.A., Kaus, B.J.P. & Schmalholz, S.M., 2011. Comparing thin-sheet models with 3-D multilayer models for continental collision, *Geophys. J. Int.,* **187,** 10–33.

Lechmann, S.M., Schmalholz, S.M., Hetenyi, G., May, D.A. & Kaus, B.J.P., 2014. Quantifying the impact of mechanical layering and underthrusting on the dynamics of the modern India-Asia collisional system with 3D numerical models, *J. geophys. Res.-Solid Earth*, **119,** doi:10.1002/2012JB009748.

Mancktelow, N.S., 1995. Nonlithostatic pressure during sediment subduction and the development and exhumation of high-pressure metamorphic rocks, *J. geophys. Res.-Solid Earth,* **100,** 571–583.

Mancktelow, N.S., 2008. Tectonic pressure: theoretical concepts and modelled examples, *Lithos,* **103,** 149–177.

Martinod, J. & Molnar, P., 1995. Lithospheric folding in the Indian Ocean and the rheology of the oceanic plate, *Bull. De La Societe Geologique De France,* **166,** 813–821.

Medvedev, S.E. & Podladchikov, Y.Y., 1999a. New extended thin-sheet approximation for geodynamic applications - I. Model formulation, *Geophys. J. Int.,* **136,** 567–585.

Medvedev, S.E. & Podladchikov, Y.Y., 1999b. New extended thin-sheet approximation for geodynamic applications - II. Two-dimensional examples, *Geophys. J. Int.,* **136,** 586–608.

Molnar, P. & Lyon-Caen, H., 1988. Some simple physical aspects of the support, structure and evolution of mountain belts, *Geol. Soc. Am. Spec. Paper*, **218,** 179–207.

Molnar, P., England, P. & Martinod, J., 1993. Mantle dynamics, uplift of the Tibetan plateau, and the Indian monsoon, *Rev. Geophys.,* **31,** 357–396.

Naliboff, J.B., Lithgow-Bertelloni, C., Ruff, L.J. & de Koker, N., 2012. The effects of lithospheric thickness and density structure on Earth's stress field, *Geophys. J. Int.,* **188,** 1–17.

Parsons, B. & Richter, F.M., 1980. A relation between the driving force and geoid anomaly associated with mid-ocean ridges, *Earth planet. Sci. Lett.,* **51,** 445–450.

Petrini, K. & Podladchikov, Y., 2000. Lithospheric pressure-depth relationship in compressive regions of thickened crust, *J. Metamor. Geol.,* **18,** 67–77.

Rubatto, D. & Hermann, J., 2001. Exhumation as fast as subduction? *Geology,* **29,** 3–6.

Schmalholz, S.M. & Podladchikov, Y.Y., 2000. Finite amplitude folding: transition from exponential to layer length controlled growth, *Earth planet. Sci. Lett.,* **181,** 617–633.

Schmalholz, S.M. & Podladchikov, Y.Y., 2013. Tectonic overpressure in weak crustal-scale shear zones and implications for the exhumation of

high-pressure rocks. *Geophys. Res. Lett.,* **40**(10), doi:10.1002/grl.50417.

Schmalholz, S.M. & Schmid, D.W., 2012. Folding in power-law viscous multi-layers, *Phil. Trans. R. Soc. A,* **370,** 1798–1826.

Schmalholz, S.M., Podladchikov, Y.Y. & Burg, J.-P., 2002. Control of folding by gravity and matrix thickness: implications for large-scale folding, *J. geophys. Res*., **107,** doi 10.1029/2001JB000355.

Schmalholz, S.M., Schmid, D.W. & Fletcher, R.C., 2008. Evolution of pinch-and-swell structures in a power-law layer, *J. Struct. Geol.,* **30,** 649–663.

Schreyer, W., 1995. Ultradeep metamorphic rocks—the retrospective viewpoint, *J. geophys. Res.-Solid Earth,* **100,** 8353–8366.

Shewchuk, J.R., 2002. Delaunay refinement algorithms for triangular mesh generation, *Comput. Geomet.-Theory Appl.,* **22,** 21–74.

Sibson, R.H., 1990. Conditions for fault-valve behavior, in *Deformation Mechanisms*, pp. 15–28, eds Knipe, R.J. & Rutter, E.H., Rheology and Tectonics.

Thomasset, F., 1981. *Implementation of Finite Element Methods for Navier-Stokes Equations*, Springer-Verlag.

APPENDIX: DERIVATION OF DEPTH-INTEGRATED FORCE BALANCE EQUATIONS

The 2-D force balance equations are

$$\frac{\partial \sigma_{xx}}{\partial x} + \frac{\partial \sigma_{xz}}{\partial z} = 0, \tag{A1}$$

$$\frac{\partial \sigma_{xz}}{\partial x} + \frac{\partial \sigma_{zz}}{\partial z} = -\rho g, \tag{A2}$$

where σ_{xx}, σ_{zz} and σ_{xz} are the components of the total stress tensor in the horizontal x-direction, vertical z-direction and the shear component, respectively, ρ is the density and g the acceleration due to gravity (Fig. A1).

The integration of eq. (A1) with respect to z yields:

$$\int_{Sb}^{St(x)} \frac{\partial \sigma_{xx}}{\partial x}\,\mathrm{d}z + \int_{Sb}^{St(x)} \frac{\partial \sigma_{xz}}{\partial z}\,\mathrm{d}z$$

$$= \int_{Sb}^{St(x)} \frac{\partial \sigma_{xx}}{\partial x}\,\mathrm{d}z + \sigma_{xz}|_{St(x)} - \sigma_{xz}|_{Sb} = 0, \tag{A3}$$

where Sb and $St(x)$ are the bottom and top integration boundaries, respectively. For the lithosphere, Sb is the compensation depth (constant in the x-direction) and $St(x)$ is the topography (variable in the
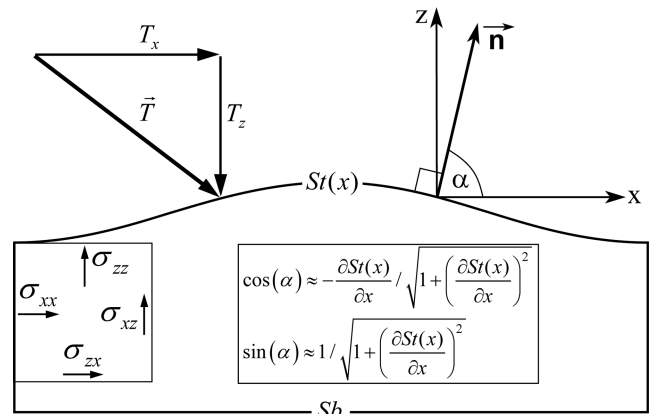

Figure A1. Sketch showing the relation between traction vector, $\vec{T}$, acting on a surface and its two components, T_x and T_z, the stress tensor components and the normal vector on the surface, $\vec{n}$, together with the approximations for the trigonometric functions sinus and cosinus.

x-direction). Next, the order of the integration and derivation operation is changed. If the integration boundary is a function of *x* then additional terms including the derivative of the integration boundary appear according to the rule of differentiation of integrals with variable integration boundaries (e.g. Bronstein *et al.* 1997). Eq. (A3) becomes

$$\frac{\partial}{\partial x}\left(\int_{Sb}^{St(x)}\sigma_{xx}\,\mathrm{d}z\right) - \frac{\partial St(x)}{\partial x}\left.\sigma_{xx}\right|_{St(x)} + \left.\sigma_{xz}\right|_{St(x)} - \left.\sigma_{xz}\right|_{Sb} = 0.$$
(A4)

Before further modifying eq. (A4), it is useful to consider the horizontal component, T_x, of the traction vector, $\vec{T}$, acting on the surface (or top integration boundary), which can be expressed by the stress tensor components at the surface using Cauchy's law (Fig. A1):

$$\left.T_x\right|_{St(x)} = \left.\sigma_{xx}\right|_{St(x)}\cos(\alpha) + \left.\sigma_{xz}\right|_{St(x)}\sin(\alpha),$$
(A5)

where α is the corresponding angle between the horizontal *x*-direction and the normal vector of the surface. Using the (differential geometry) approximations for $\cos(\alpha)$ and $\sin(\alpha)$ given in Fig. A1 yields for T_x on the surface $St(x)$

$$\left.T_x\right|_{St(x)} = -\left.\sigma_{xx}\right|_{St(x)}\frac{\partial St(x)}{\partial x}\bigg/\sqrt{1+\left(\frac{\partial St(x)}{\partial x}\right)^2}$$

$$+ \left.\sigma_{xz}\right|_{St(x)}\bigg/\sqrt{1+\left(\frac{\partial St(x)}{\partial x}\right)^2}.$$
(A6)

Using the above expression (A6) in eq. (A4) yields

$$\frac{\partial}{\partial x}(\bar{\sigma}_{xx}) = -\left.T_x\right|_{St(x)}\sqrt{1+\left(\frac{\partial St(x)}{\partial x}\right)^2} + \left.\sigma_{xz}\right|_{Sb},$$
(A7)

where the overbar, $\bar{\sigma}_{xx}$, indicates the vertical integral of the horizontal total stress. Quantities with overbar have units of Pa·m or N m^{-1} (Table 1). For the considered lithospheric conditions the tractions, $\vec{T}$, are zero at the free surface and hence also their horizontal components, T_x, are zero. Furthermore, both the isostatic compensation condition discussed in the analytical models, and the free-slip condition used in the numerical models require $\left.\sigma_{xz}\right|_{Sb} = 0$. Therefore, eq. (A7) reduces to

$$\frac{\partial}{\partial x}(\bar{\sigma}_{xx}) = 0.$$
(A8)

Eq. (A8) corresponds to the equation presented in Molnar & Lyon-Caen (1988). In contrast, Naliboff *et al.* (2012) argue that terms with the horizontal derivative of the topography (here the surface $St(x)$) should be present in the depth-integrated horizontal force balance if topographic slopes are not sufficiently gentle, which is, however, incorrect for a stress-free surface. Our results show that horizontal derivatives of the topography always vanish if the topography is described by a stress-free surface, no matter how large the slope of the topography is. A detailed derivation of the depth-integrated balance equations for the general 3-D case is given in Medvedev & Podladchikov (1999a).

Integration of the vertical projection of the force balance eq. (A2) gives

$$\int_z^{St(x)}\frac{\partial\sigma_{xz}}{\partial x}\,\mathrm{d}z' + \int_z^{St(x)}\frac{\partial\sigma_{zz}}{\partial z}\,\mathrm{d}z' = -P_L(x,z).$$
(A9)

Note that we use *z* as the lower limit of integration here. Derivations similar to (A3)–(A8) applied to eq. (A9) result in (see also Medvedev & Podladchikov 1999a):

$$\sigma_{zz}(x,z) = -P_L(x,z) - Q(x,z),$$
(A10)

where Q is a measure of the shear stress contribution in the vertical force balance with

$$Q(x,z) = \frac{\partial}{\partial x}\int_z^{St(x)}\sigma_{xz}\,\mathrm{d}z'.$$
(A11)

Eq. (A10) can be rewritten in several useful forms using $\sigma_{zz} = -P + \tau_{zz}$ and $\tau_{zz} = -\tau_{xx}$:

$$\tau_{zz} = P - P_L - Q = P_O - Q,$$

$$P_O = \tau_{zz} + Q = -\tau_{xx} + Q.$$
(A12)

The integration of eqs (A10) and (A12) over the thickness of the lithosphere does not change the equalities, and thus the same equations are valid for 'overbarred' terms.

The above equations are exact if there is no shear stress at the base, which is assumed by the compensation condition at *Sb*. We now estimate the inaccuracy of the thin sheet approximations, which assume local isostasy at *Sb* and neglect the shear stress in the force balance. At the compensation depth *Sb*, eq. (A10) becomes:

$$Q(x,Sb) = \frac{\partial}{\partial x}(\bar{\sigma}_{xz}) = -\sigma_{zz}(x,Sb) - P_L(x,Sb).$$
(A13)

The compensation condition assumes a layer of negligible strength around *Sb*, and, therefore, negligible deviatoric stresses within the underlying layer, and yields:

$$-P(x,Sb) = \sigma_{xx}(x,Sb) = \sigma_{zz}(x,Sb)$$

$$\sigma_{xz}(x,Sb) = 0, \quad \frac{\partial\sigma_{xz}}{\partial z}(x,Sb) = 0.$$
(A14)

To fulfil the compensation condition a layer of negligible strength is necessary because also the vertical derivative of the shear stress must be zero. A free-slip condition at *Sb*, that is, zero shear stresses along *Sb*, is not sufficient to guarantee a constant pressure along *Sb*. Eq. (A14) can be used to replace $\sigma_{zz}(x,Sb)$ by $-P(x,Sb)$ in eq. (A13) yielding:

$$Q(x,Sb) = P(x,Sb) - P_L(x,Sb) = P_O(x,Sb).$$
(A15)

The tectonic overpressure at *Sb* and at a certain horizontal position *x* depends on the horizontal gradient of the shear stresses integrated vertically across the entire lithosphere. If $P_O(x,Sb)$ is zero then $\bar{\sigma}_{xz}$ is constant along the lithosphere. Eq. (A15) also indicates that a tectonic overpressure can exist at the model base although all deviatoric stresses are zero at the base, because the tectonic overpressure is related to the shear stress integrated over the entire depth of the model.

Combining eq. (A14) and the horizontal force balance (A1) at the compensation depth reveals that σ_{zz} is a constant along *Sb*:

$$\frac{\partial\sigma_{xx}}{\partial x} = \frac{\partial\sigma_{zz}}{\partial x} = 0.$$
(A16)

From eqs (A13) and (A15) the difference, Δ, between mountains and lowlands at *Sb* then becomes (considering $\Delta\sigma_{zz} = 0$ from A16):

$$\Delta Q = \Delta\left(\frac{\partial}{\partial x}\bar{\sigma}_{xz}\right) = -\Delta P_L = \Delta P_O.$$
(A17)

Eq. (A17) is in contrast with the local isostasy condition, which assumes $P_L = \text{const}$. Thus, the deviation from isostasy ΔP_L at *Sb* is

directly related to the difference in the horizontal derivative of the integrated shear stresses, which corresponds to a flexural moment (Medvedev & Podladchikov 1999a). A consequence of eq. (A17) is that an inviscid layer at the base of the lithosphere does not guarantee isostasy, because isostasy requires that horizontal gradients of $\bar{\sigma}_{xz}$ are zero.

To complete the horizontal force balance for the thin sheet approximation, eq. (3) or (A8) requires the estimation of the pressure from eq. (A12). Usually, the shear stress term Q (or $\bar{Q}$) was assumed to be zero and dropped from the integrated vertical force balance in the traditional thin sheet approximations (the exception is the extended thin sheet approximation of Medvedev & Podladchikov 1999a) resulting in the approximate equivalence between the vertical total stress and the lithostatic pressure, that is, $\sigma_{zz}(x, z) \approx -P_L(x, z)$. This simplification however is not obvious. Ghosh *et al.* (2009) suggested dropping the term Q in eq. (A10) where naturally $P_L \gg Q$ on the crustal or lithospheric scales. However, this inequality does not allow dropping Q from eq. (A12), the main equations used in the derivation of thin sheet equations.

Also, the force balance equations do not include absolute values of shear stresses but gradients of shear stresses. Gradients of shear stresses can be large although absolute values of shear stresses are small. Consequently, the potentially small value of shear stresses in the lithosphere is not a sufficient argument to neglect shear stresses in the force balance equations because also gradients of shear stresses should be small. Medvedev & Podladchikov (1999b) demonstrated that Q cannot be dropped for some special cases. The traditional thin sheet approximations (e.g. England & McKenzie 1982) used a qualitative reasoning to drop Q without a quantitative analysis. Here, we test the importance of Q with numerical simulations for the configurations displayed in Fig. 1. In particular, we test if $P_O \approx -\tau_{xx} = \tau_{zz}$ which is valid only if $Q \ll P_O$ (eq. A12).

The analysis of this section can be extended to the 3-D case without significant changes in relations between the components of the stress field. Applications of those 3-D equations to a (quasi-) 2-D case and use of correct definitions of mechanical terms naturally would not change the conclusions of our study (*cf.* Ghosh *et al.* 2009).